



Mathematisch-Naturwissenschaftliche Fakultät
Ernst-Moritz-Arndt-Universität Greifswald

Diplomarbeit

Spectroscopic data for astrophysics

Robert Warmbier
Greifswald, 29.04.2008

Gutachter:
PD Dr. Ralf Schneider
Prof. Dr. Peter Hauschildt, Universität Hamburg

Table of Contents

Table of Contents	iii
Zusammenfassung	v
1 Introduction	1
2 Basics	3
2.1 Methane	3
2.2 Quantum mechanics	5
2.2.1 Born-Oppenheimer approximation	5
2.2.2 Hartree-Fock theory	5
2.2.3 Dipole moment	6
2.2.4 Harmonic oscillator	7
2.3 Coordinate systems	8
2.4 Subsumption	8
3 Tools and methods	9
3.1 Potential energy and dipole moment surface	9
3.1.1 <i>Ab initio</i> quantum chemistry	9
3.1.1.1 Coupled Cluster method	10
3.1.1.2 Configuration Interaction	10
3.1.1.3 Averaged Coupled Pair Function	11
3.1.2 Representation and Properties	11
3.1.3 Elements of the algorithm for the generation of spectroscopic data	13
3.2 Multimode	14
3.2.1 Virtual Configuration Interaction	14
3.2.2 Watson-Hamiltonian	15
3.2.3 Adiabatic rotation approximation	16
3.2.4 Elements of the algorithm for the generation of spectroscopic data	17
3.3 Calculation of spectroscopic data	18
3.3.1 State analysis	18
3.3.2 Dipole moment matrix	21
3.3.3 Einstein coefficients	23
3.3.4 Elements of the algorithm for spectroscopic data	24
3.4 Summary of the algorithm	25
4 Results	27
4.1 Tests	27
4.1.1 PES properties	27
4.1.2 Harmonic oscillator	32
4.1.3 Morphing	34
4.1.4 Convergence	36

Table of Contents

4.1.5	Computational effort	37
4.2	Rotational dependence for energies and dipoles	41
4.3	Einstein coefficients	42
4.4	Spectra	44
4.4.1	Comparison of $J = 0$ lines for different evaluation methods	44
4.4.2	Spectra for different temperatures	46
4.4.3	Comparison with HITRAN	47
4.5	Astrophysical application	48
4.5.1	Perspective and improvements	49
5	Conclusion	51
	Bibliography	53
	Acknowledgements	57

Zusammenfassung

Spektroskopische Daten sind wichtig für die Astrophysik, weil die einzig verfügbare Observable Licht der verschiedenen Wellenlängen ist. Das Wissen um die Spektren aller Materiearten, die gemessen werden, ist daher kritisch für die Auswertung der Beobachtungen. Neben Elementarteilchen und Atomen sind Kohlenwasserstoffe häufig anzutreffen. Sie stammen aus dem Inneren alter Sterne, die unter anderem auch Kohlenstoff durch Fusion erzeugen. In ihren relativ kalten Atmosphären können sich dann Kohlenwasserstoffe bilden. Weiterhin finden sich diese auch in den Atmosphären von Gasriesen und im interstellaren Medium. Methan ist der mit Abstand häufigste Vertreter von Kohlenwasserstoffen.

Die bisherigen Datensammlungen von spektroskopischen Daten von Kohlenwasserstoffen bestehen aus Datensätzen unterschiedlichster Herkunft und Genauigkeit. Dies führt bei der Integration in Rechenpaketen zum Strahlungstransport zu falscher Physik und kann zu numerischen Instabilitäten führen.

Das Ziel dieser Arbeit ist es daher eine spektroskopische Datenbank für Methan zu erstellen, die alle Rotations-Vibrations-Übergänge bis zu einer maximalen Energie der oberen Zustände erfasst. Diese beträgt 6200 cm^{-1} was zirka 9000 K entspricht. Dabei liegt der Hauptaugenmerk auf der Konsistenz der erhaltenen Daten unter Inkaufnahme eingeschränkter Qualität einzelner Linien.

Dazu wurden ausgehend von *ab initio* Daten globale Hyperflächen der potentiellen Energie und des Dipolmomentes in Abhängigkeit von der molekularen Konfiguration erstellt. Diese Oberflächen erlauben eine schnelle, aber trotzdem genaue Lösung der Schrödinger Gleichung. Mit Hilfe der verwendeten Codes konnten exakte Rotations-Vibrations Energien gewonnen werden, die eine hinreichende Genauigkeit für die astrophysikalische Anwendung besitzen. Desweiteren sind Dipolmatrixelemente zu berechnen, was aufgrund der technischen Einschränkungen der verwendeten Codes nur auf Vibrations-Niveau mit genäherter Rotationsabhängigkeit möglich war. Aus diesen Daten konnten dann Einsteinkoeffizienten errechnet werden, die ein Maß für die quantenmechanische Übergangswahrscheinlichkeit pro Molekül pro Sekunde sind.

Vergleiche mit existierenden Datenbanken bestätigen trotz aller benutzter Näherungen die Qualität der Ergebnisse und definieren damit die Möglichkeit mit dieser Vorgehensweise auch andere Moleküle zu behandeln. Durch weitergehende Verbesserungen im benutzten Algorithmus, die allerdings den Rahmen einer Diplomarbeit sprengen würden, ist eine Ausdehnung auf spektroskopische Anwendungen mit erhöhten Genauigkeitsansprüchen möglich.

Zusammenfassung

Chapter 1

Introduction

Spectroscopic data are important for astrophysics because the only available observable is usually light, electro-magnetic radiation of any frequency. Therefore, the knowledge of spectra of all particles measured is critical for the evaluation of the observations. Besides elementary particles hydrocarbons are very often measured. This is because carbon, which is formed in stars via fusion, is quite reactive and bonds with hydrogen are relatively stable. The cold atmospheres of old stars, for example brown dwarfs [2], accommodate various kinds of molecules including hydrocarbons. Gas giants can also consist mainly of hydrocarbons, the outer planets of our solar system are examples of it. Furthermore, the interstellar space is filled with material from nova explosions which form clouds and nebula, also including hydrocarbons. The most common representative is methane.

Radiation transport calculations are therefore important for understanding experiments and basic physics studies. Essential elements for such calculations are spectroscopic databases like HITRAN [3, 4]. These databases are patched from different sources, experiments and theory. Therefore, the data is inconsistent at interfaces. This is a source for wrong physics and may cause numerical problems during integration.

To obtain spectroscopic data of hydrocarbons with one single method and deliver a consistent dataset is the task of this work. The quality of each single line is of secondary interest, because deviations will partly be canceled through integration. Also the experimental data in astrophysics is of quite low accuracy, because hydrocarbon radiation has a low intensity and therefore uncertainties of 20 to 30% are existing in experimental data. Hence, a general method for obtaining spectroscopic data is developed in this work with methane as an example and a complete dataset of all possible rovibrational lines of methane up to an initial state energy of 6200 cm^{-1} ($\approx 8920 \text{ K}$) is calculated with a relative error for energy levels of about 1%.

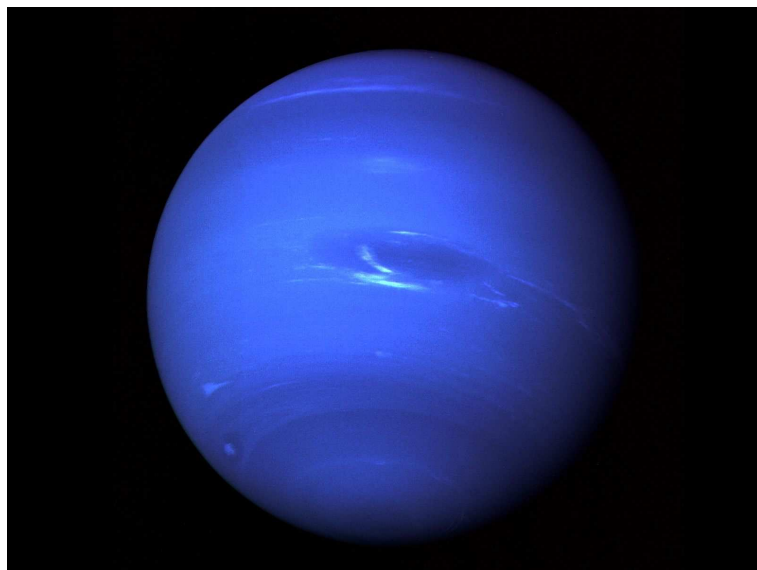


Figure 1.1: Picture of Neptune, a gas giant with a relatively high fraction of methane [1].

Hydrocarbons are also important for other fields of physics. Low temperature hydrocarbon plasmas are of interest e.g. for diamond-like coatings. In fusion devices carbon is often used as divertor material. There, plasma-wall interactions of the hydrogen plasma and the carbon wall produce hydrocarbons[5, 6, 7, 8]. To expand the usability of the spectral data obtained by the method used in this work to these fields of physics, their accuracy should be as high as possible. Hence, possible improvements of the methods are also discussed.

Chapter 2 provides basic information on methane and quantum physics. Chapter 3 will describe the tools and methods used in this work. The basic algorithm from *ab initio* quantum chemistry data to the complete spectroscopic information is developed. The results, beginning with diagnostics of the underlying potential energy surface fit are presented in chapter 4. The quality of the potential energy surface determines the overall quality limitation of all further calculations. The final database is presented as well as an example application for astrophysics.

At the end a conclusion of the work is given, including an evaluation of the benefits and limits of the method used in this work.

Chapter 2

Basics

The molecule chosen as test example in this work - for the general procedure developed - is methane, because it is the most common hydrocarbon in stellar and planetary atmospheres as mentioned before. Therefore, a characterization of methane is presented at the beginning of this chapter. Afterwards some basics of quantum mechanics are introduced, which are needed to understand the specific approaches used later in this work.

2.1 Methane

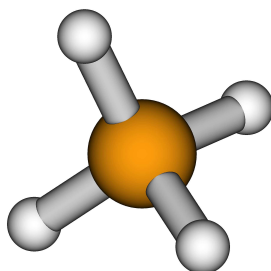


Figure 2.1: Equilibrium configuration of methane

Methane is a hydrocarbon of the group of alkanes with the formula CH_4 . It is a colorless, odorless gas under normal conditions. The 4 hydrogen atoms are placed equally around the carbon atom in the ground state (see figure 2.1). Methane has non-polar covalent binding and is quite nonreactive, except with halogens like fluorine, chlorine, etc. With these elements it undergoes substitution reactions, called halogenation. A list of physical and chemical properties is given in table 2.1.

To understand the spectroscopic properties of methane the knowledge of different vibrational modes of the molecule is important. Methane is a highly symmetric spherical top molecule belonging to the T_D point group and has 9 vibrational degrees of freedom. Due to the high symmetry they degenerate to 4 distinguishable modes. The non-degenerated representation is labeled with v_1 to v_9 , the numbers are ordered by increasing energy. The degenerated representation is written as n_1 to n_4 .

The n_1 mode is not degenerated and corresponds to v_6 . It is a symmetric stretch mode (figure 2.2 a) at 2916.5 cm^{-1} [10] ($1000 \text{ cm}^{-1} = 0.1240 \text{ eV}$). The mode n_2 is a twofold degenerated torsional bend mode (figure 2.2 b) corresponding to the modes v_4 and v_5 . The first excitation level is at 1533.3 cm^{-1} [10]. The n_3 mode is threefold degenerated corresponding to v_7 to v_9 . The

Table 2.1: Table of physical and chemical properties of methane.

Property	Value
C-H bond length	2.06Bohr = 0.109nm
Bond angle	109.5°
Molecular weight[9]	16.043 g/mol
Melting point[9]	-182.5 °C
Liquid density (1.013 bar at boiling point)[9]	422.62 kg/m ³
Boiling point (1.013 bar)[9]	-161.6 °C
Critical temperature[9]	-82.7 °C
Critical pressure[9]	45.96 bar
Gas density (1.013 bar at boiling point)[9]	1.819 kg/m ³
Gas density (1.013 bar and 15 °C)[9]	0.68 kg/m ³
Autoignition temperature[9]	595 °C

asymmetric stretch (figure 2.2 c) has an energy of 3019.5 cm^{-1} . The second threefold degenerated mode n_4 is an umbrella bend mode (figure 2.2 d). It corresponds to the modes v_1 to v_3 and has an energy of 1310.8 cm^{-1} .

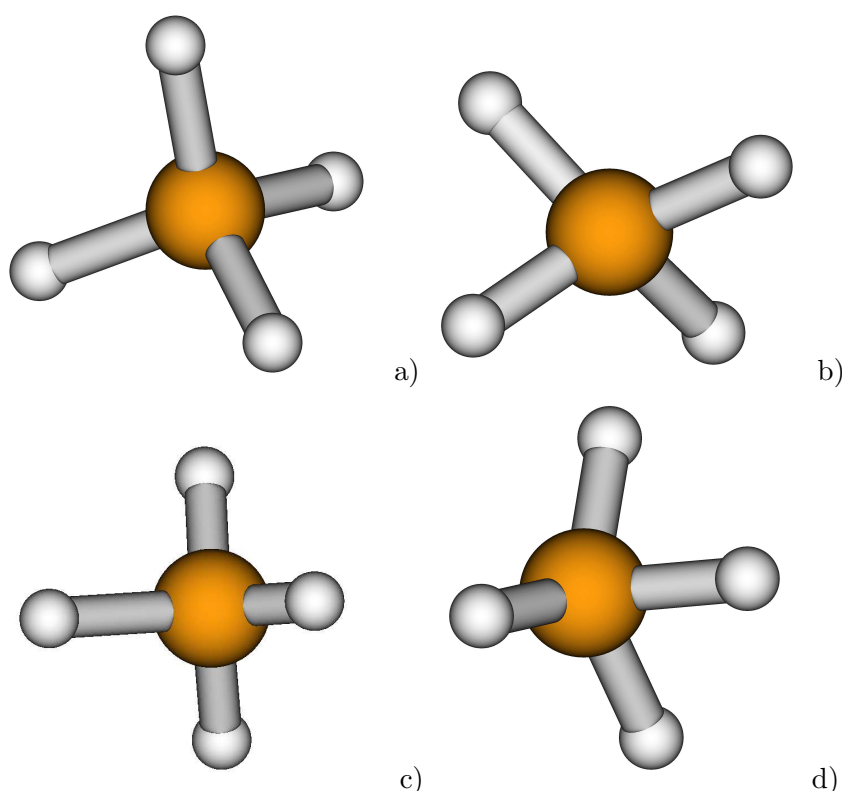


Figure 2.2: a) symmetric stretch (n_1), b) torsional bend (n_2), c) asymmetric stretch (n_3), d) umbrella bend (n_4)

These vibrational modes can produce non-zero dipole moments, which determine the transition probabilities and eventually the spectroscopic properties. The dipole operator of methane is of symmetry A_2 for all three components, therefore transitions are only allowed, if the direct product of symmetry operators of two states contain A_2 . This is true for modes n_3 and n_4 which are infrared (IR) active.

2.2 Quantum mechanics

A necessary prerequisite for this work is the calculation of rotational and vibrational states and their energies. In a molecular system a general approach for a Hamiltonian include five terms: The kinetic parts for nuclei (N) and electrons (e), the nuclid-nuclid interaction, the electron-electron interaction and one term taking into account the interaction between nuclei and electrons.

$$\hat{H} = \hat{T}_N(\mathbf{R}) + \hat{T}_e(\mathbf{r}) + \hat{V}_{eN}(\mathbf{r}, \mathbf{R}) + \hat{V}_{NN}(\mathbf{R}) + \hat{V}_{ee}(\mathbf{r}). \quad (2.1)$$

The correlation between electrons and nuclei prevents the separation of the electronic and the nuclid problem. An analytical solution of the Schrödinger equation is only possible for a very small number of simplistic problems, like 2-body problems (e.g. hydrogen). Approximations have to be done to solve systems having several atoms. To make things treatable the Born-Oppenheimer approximation (see 2.2.1) is introduced, allowing the separation of the electronic and the nuclei problem, which will be summarized in the next section. Afterwards, it is shown how the Hartree-Fock approximation, described in 2.2.2, allows the solution of the electronic problem. The general idea for a handy Hamiltonian is to have a potential depending on the positions of electrons with the coordinates of the nuclei as parameters. This delivers an effective electronic potential for specific nuclid orientations (see section about potential energy surface (3.1)). This potential, using a fitted expression, can be used to calculate molecular rotations and vibrations in the 'electronic' potential. While Hamiltonians and potentials are needed to calculate energies, spectroscopic analysis also needs dipole data (see 2.2.3) and therefore the dipole moment operator is shortly discussed. Finally, in 2.2.4 the basics of the quantum mechanics of harmonic oscillators is introduced, because this is needed as background information for the quantum dynamical analysis of oscillations of molecules, which are important to understand their spectrum. For a realistic description of molecular oscillations, the choice of coordinates for this work is presented in 2.3.

2.2.1 Born-Oppenheimer approximation

The Born-Oppenheimer approximation [11, 12, 13, 14] was introduced 1927 by Oppenheimer and Born [15] to give an appropriate description of the Hamiltonian of molecules which is still treatable. The energy terms can be arranged by orders of $\sqrt{m/M}$, where m is the electron mass and M the average nuclid mass, with a mass difference between electrons and nuclids (protons) of about 1836 times. Due to the large inertia difference one may assume that electrons follow the movement of nuclei instantaneously. The nuclei coordinates are then parameters for electronic movements. The Born-Oppenheimer approach allows us to separate the electronic and the nuclid problem. So one can solve the electronic problem with the positions of the nuclei as parameters and use these results for solving the full problem.

2.2.2 Hartree-Fock theory

The Hartree approximation was formulated by Hartree in 1928. It is assumed, that in a many-body system every electron is affected not only by the core potential but in addition by an effective potential of all other electrons.[13, 14] This allows to represent every electron with a one-body wave function

$$\varphi_i = \phi_i(\mathbf{x}_i)\chi_i(m_{s_i}), \quad (2.2)$$

which is a product of spatial and spin functions. The one-body Schrödinger equations are coupled through the effective potential and depend therefore on the wave functions of the other

electrons. Due to this, the wave functions have to be solved self consistently with an iterative method. The many-body wave function is constructed as a product wave function

$$\Psi(1, \dots, N) = \varphi_1(1) \dots \varphi_N(N). \quad (2.3)$$

This wave function is not antisymmetric and additional restrictions have to be made to satisfy the Pauli principle. The one-body states have to be different and orthogonal.

The wave function for a system of fermions has to be antisymmetric to the exchange of neighboring indices. Due to the limitations of the Hartree approximation Fock and Slater independently proposed to use an antisymmetrized sum of all orbitals, which can be obtained by simply interchanging labels. The most common representation is the so-called Slater determinant

$$\Psi(1, \dots, N) = \frac{1}{\sqrt{N!}} \begin{vmatrix} \varphi_1(1) & \dots & \varphi_1(N) \\ \vdots & & \vdots \\ \varphi_N(1) & \dots & \varphi_N(N) \end{vmatrix}. \quad (2.4)$$

In this Hartree-Fock approximation an additional, non-local, term is introduced into the Hamiltonian, called exchange interaction [13, 14]. This is an effect of quantum mechanics which corresponds to the Pauli principle, saying that quantum mechanical particles with same spin orientation are indistinguishable.

The way of getting the best Hartree-Fock energy and/or wave function is the iterative self consistent field (SCF) method. One starts with an initial guess for the orbitals, for example hydrogen functions. Then, one solves the eigenvalue problem iteratively until convergence is reached.

The major shortcoming of this method is the use of an averaged interaction for electrons neglecting the correlation energy, which is defined as the difference between the exact non-relativistic energy and the Hartree-Fock energy. While Pauli repulsion of electrons with identical spin orientation is already given by the exchange interaction, the direct instantaneous Coulomb interaction between electrons can not be represented by an averaged field, leading to the missing correlation energy. Methods which try to include the correlation energy are called post-Hartree-Fock methods.

2.2.3 Dipole moment

The dipole moment of a point charge is defined as

$$\mathbf{d} = q \cdot \mathbf{r}. \quad (2.5)$$

For several point charges a summation over the one-body terms, meaning the term for one single point charge without reckoning other charges, has to be done. In case of space charges an integration over the charge density, replacing the charge, is done. In quantum mechanics the expectation value of the dipole moment operator is defined by $M_{ij} = \langle \Psi_i | \mathbf{d} | \Psi_j \rangle$ [16, 12, 14]. This is also the definition of the electronic transition probability between these states. This can be seen easily, if one interprets the dipole moment as a perturbation allowing transitions. The effective dipole moment of molecules are defined by nuclei and electrons, where the nuclei can be considered as localized. The electronic part of the dipole moment has to be calculated from the quantum mechanical probability density in dependence of the nuclei configuration.

For the equilibrium configuration of methane the hydrogen atoms are placed equally around the carbon atom as displayed in figure 2.1. Therefore the nuclid part has a zero dipole moment. The C-H bonds are covalent, meaning that the valence electrons have their highest probability density between the two nuclei. Therefore the electronic configuration is also symmetric causing a zero total dipole moment. Vibrational motion produces temporary effective dipole moments allowing excitations, for example of rotational modes. As a consequence, the understanding of

the dynamics of the molecule is needed for a proper calculation of dipole moments. Vibrational modes with symmetric displacements q_i produce no effective dipole moment $\frac{\partial \mathbf{d}}{\partial q_i} = 0$ and are therefore not infrared active. Excitations of these modes can occur by external stimulation like electron scattering. These modes are therefore visible in Raman spectra [17]. Asymmetric modes do have $\frac{\partial \mathbf{d}}{\partial q_i} \neq 0$ and are infrared active.

2.2.4 Harmonic oscillator

The simplest possible type of oscillation is the harmonic oscillator. Following the notation of Schwabl[13] the corresponding stationary Schrödinger equation is ($p = -i\hbar \frac{\partial}{\partial q}$)

$$\left[-\frac{\hbar^2}{2m} \nabla^2 + \frac{m\omega^2 q^2}{2} \right] \Psi(q) = E\Psi(q). \quad (2.6)$$

The solution of this equation is based on Hermite polynomials. The eigenvalues are

$$E_n = \hbar\omega(n + 1/2). \quad (2.7)$$

A shorter way to solve the problem is via Hermitean operators. One defines two Hermitean ladder operators as follows:

$$\begin{aligned} a &= \frac{\omega m q + ip}{\sqrt{2\omega m \hbar}} \\ a^\dagger &= \frac{\omega m q - ip}{\sqrt{2\omega m \hbar}} \end{aligned} \quad (2.8)$$

with $[a, a^\dagger] = 1$. In this notation the Hamiltonian is

$$\hat{H} = \frac{1}{2} \hbar\omega (a^\dagger a + a a^\dagger). \quad (2.9)$$

A comparison with equation 2.7 and the usage of the commutator relation leads to

$$H = \hbar\omega \left(a^\dagger a + \frac{1}{2} \right) = \hbar\omega \left(\hat{n} + \frac{1}{2} \right) \quad (2.10)$$

with $\hat{n} = a^\dagger a$ is the occupation number operator. The wave function also can be expressed by the raising operator

$$\begin{aligned} \Psi_n &= \frac{1}{\sqrt{n!}} (a^\dagger)^n \Psi_0 \\ \Psi_0 &= (\sqrt{\pi} q_0)^{-1/2} \exp -\frac{1}{2} \left(\frac{q}{q_0} \right)^2. \end{aligned} \quad (2.11)$$

q_0 is the characteristic length and is defined as $q_0 = \sqrt{\hbar/m\omega}$.

In molecules vibrations with harmonic and with anharmonic potentials occur. The harmonic oscillator can be used as a linear approximation even for anharmonic oscillators, because for very small energies/ displacements the deviation from the harmonic behavior is relatively small. Figures 4.6 and 4.7 in section 4.1.2 show both cases.

The single excitation of an oscillator is called fundamental, higher excitations are called overtones. Transitions from an energetic higher excitation level to a lower one release photons. The lines in the electromagnetic spectrum belonging to transitions with the same higher and lower vibrational levels are called bands.

2.3 Coordinate systems

The most common coordinate system is the Cartesian system with 3 orthogonal basis vectors. In principle, every problem can be expressed in these coordinates. For a N -body system $3N$ coordinates are needed to describe the system. The use of a set of generalized coordinates is possible and simplifies the problem as derived in classical Hamiltonian mechanics [18].

Another possibility is to use the internuclear distances, where the number of coordinates is $N(N - 1)/2$. The number of independent coordinates depends on the symmetry of the system. External potentials can not be described within this basis set, on the other hand the usages of symmetries and invariants is comfortable.

The coordinate system used for most of the calculations in this work are normal coordinates. A N -body system has $3N$ degrees of freedom, including 3 translational directions for the center of mass and 3 rotational modes along some axis defined by the structure of the molecule. This leaves $3N - 6$ degrees of freedom for vibrational motions of the molecule in which the center of mass is not moving. There is one exception for linear molecules where only two rotational axes exist, increasing the number of vibrational degrees of freedom to $3N - 5$. For molecules it is reasonable to define coordinates along the displacement vectors of the vibrational modes. Hence the $3N - 6$ classical independent modes are called normal modes and the set of coordinates relying on them are called normal coordinates. Symmetries causing degeneracy of normal modes lead to orthogonal normal coordinates, but symmetry is not conserved automatically by these coordinates.

2.4 Subsumption

In this chapter some of the basic physics was introduced. The methane molecule, which is studied in this thesis, was characterized. The basic approximations for solving the molecular Schrödinger equation were pointed out. The dipole moment, which is the background for spectroscopic calculations was explained. In addition, an introduction to the coordinate systems used in this work was given.

Chapter 3

Tools and methods

This chapter gives an overview of the tools used in this work. Already existing codes were used for most of the calculations, but in addition new programs for the evaluation of results had to be developed. As mentioned before the main task of this work was to obtain spectroscopic data of methane for astrophysics. The algorithm developed for this should also allow the calculation of spectroscopic data for other hydrocarbons without conceptual changes. For this algorithm, several elements are needed. First the potential energy and dipole hypersurfaces used in this work are explained. They deliver the electronic potential and dipole moments for the calculations with the MULTIMODE package, which is discussed thereafter. This package provides rovibrational energies and transition matrix elements. Then the tools developed for obtaining the final spectroscopic data are explained as well as the general algorithm used. The individual elements of the algorithm for calculating spectroscopic data will be highlighted at the end of each section.

3.1 Potential energy and dipole moment surface

A molecular potential energy surface (PES) is a hypersurface of the electronic potential depending on the nuclei configuration. Normally this surface only includes the electronic ground state which restricts the usage to pure rotational/vibrational systems. The global minimum of this surface corresponds to the equilibrium geometry of the molecule. While the potential is a scalar and the functional dependency of the hypersurface can be described using a basis set of internuclear distances, the dipole moment surface (DMS) requires a different choice of coordinates. This is because the dipole moment is a vector quantity and therefore not invariant under translations. Due to this, it can not be described by internuclear distances and Cartesian coordinates have to be used.

To obtain a PES one has to calculate a large number of potential energy values for different configurations and then run a fitting procedure to determine the dependency of the PES. Normally, post-Hartree-Fock methods are used to obtain the *ab initio* data. The specific methods used in this work for the production of adequate data and fitting of the PES are explained below. The quality of the PES is more critical for the spectroscopic results than the DMS, because the potential influences the wave function and the final energy directly, while the dipole moment has only influence on the transition matrix $M_{ij} = \langle \Psi_i | \mathbf{d} | \Psi_j \rangle$. This matrix, however, is again strongly determined by the wave functions.

3.1.1 *Ab initio* quantum chemistry

There are several post Hartree-Fock methods available for solving the Schrödinger equation to get the full energy of the electronic problem. The PES used in this work is fitted from *ab initio* calculations employing restricted coupled cluster method with singles and doubles and perturbative treatment of triples [RCCSD(T)] with augmented cc-pvtz basis, which will be explained in the following section. Because the DMS was calculated with the averaged coupled pair functional [ACPF] with cc-pvtz basis, this will be shortly summarized afterwards. All *ab initio* calculations have been done with the MOLPRO 2006 package [19].

3.1.1.1 Coupled Cluster method

The coupled cluster method is a single reference *ab initio* method for calculations of molecular electronic energies. It uses a wave function which is constructed from the Slater-determinant Ψ_0 and some excitation operators \hat{T} in an exponential form. Single reference means, that at the Hartree-Fock level only one Slater-determinant is used.

$$\Psi_{CC} = \exp(\hat{T})\Psi_0, \quad (3.1)$$

where $\hat{T} = \hat{T}_1 + \hat{T}_2 + \hat{T}_3 + \dots + \hat{T}_n$ is a linear combination of all n-type excitations

$$\begin{aligned} \hat{T}_1\Psi_0 &= \sum_i \sum_a C_i^a \Psi_i^a \\ \hat{T}_2\Psi_0 &= \sum_{i>j} \sum_{a>b} C_{ij}^{ab} \Psi_{ij}^{ab} \\ &\text{and so on.} \end{aligned} \quad (3.2)$$

Putting equation 3.2 into 3.1 delivers the CCSD wave function with

$$\Psi_{CCSD} = \Psi_0 + \sum_a \sum_i C_i^a \Psi_i^a + \sum_{i>j} \sum_{a>b} C_{ij}^{ab} \Psi_{ij}^{ab} + \sum_{ab} \sum_{ij} C_i^a C_j^b \Psi_{ij}^{ab} + \text{higher order terms.} \quad (3.3)$$

The letters S,D and T refer to single, double and triple excitations. The advantage of CC theory is that the higher excitations are included, but their coefficients are determined by the lower order excitations. The coefficients are determined by projecting Schrödinger's equation on the left with the configurations generated by the \hat{T} operator. This replaces the eigenvalue problem by a non-linear simultaneous system, requiring iterative solution, which converges fast in most cases. CCSD provides a size-extensive and accurate description of electron correlation effects for non-degenerate ground states of molecules near the equilibrium geometries with computer costs that enable routine calculations for systems with up to 50-100 correlated electrons and a few hundred basis functions. CCSDT scales as N^8 which is impractical for all but the simplest of systems. A more practical alternative is CCSD(T) where the effect of triples is estimated through perturbation theory with a non-iterative N^7 cost. With a sufficient large basis set CCSD typically recovers 95% of the correlation energy for a molecule at equilibrium geometry, while CCSDT (triple excitation included) gives rise to further five- to ten-fold reduction in error[20]. With such accuracy the coupled cluster method is the method of choice for accurate small-molecule calculations.[5]

In the restricted CCSD theory (RCCSD) certain restrictions among the amplitudes are introduced, such that the linear part of the wave function becomes a spin eigenfunction[19].

3.1.1.2 Configuration Interaction

The configuration interaction method (CI) [21] is a linear variational method for solving the nonrelativistic many-electron Schrödinger equation. The term 'configuration' describes the linear combination of Slater determinants used for the wave function. In terms of a specification of orbital occupation, interaction means the mixing of different electronic configurations. Due to the long CPU time and immense hardware required for CI calculations, the method is limited to relatively small systems. In order to account for electron correlation, CI uses a variational wave function that is a linear combination of configuration state functions (CSFs) built from spin orbitals (denoted by the superscript SO),

$$\Psi = \sum_{I=0} c_I \Phi_I^{SO} = c_0 \Phi_0^{SO} + c_1 \Phi_1^{SO} + \dots \quad (3.4)$$

where Ψ is usually the electronic ground state of the system. If the expansion includes all possible CSFs of the appropriate symmetry, then this is a full configuration interaction procedure which exactly solves the electronic Schrödinger equation within the space spanned by the one-particle basis set. The first term in the above expansion is normally the Hartree-Fock determinant. The other CSFs can be characterized by the number of spin orbitals that are swapped with virtual orbitals from the Hartree-Fock determinant. The method CISD is limited to single and double excitations. Single excitations on their own do not mix with the Hartree-Fock determinant. The multi-reference configuration interaction method consists in a configuration interaction expansion of the eigenstates of the electronic molecular Hamiltonian in a set of Slater determinants which correspond to excitations of the ground state electronic configuration but also of some excited states. The Slater determinants from which the excitations are performed are called reference determinants.

3.1.1.3 Averaged Coupled Pair Function

The averaged coupled pair function was introduced first by Gdanitz and Ahlrichs in 1988 [22]. It is a modification of the multi-reference CI(SD) method. Its advantage is the easy implementation and simplicity. The first version of ACPF had the tendency to overestimate the effect of higher than double substitutions. In addition, it generated some instability for a bad zero-order wave function guess in some special cases. In 2001 Gdanitz and Ahlrichs [23] published an improved version of ACPF. This version is stable and almost as good as CCSD but much faster. Therefore, this method is a good choice for *ab initio* dipole moment calculations for which perfect accuracy is not necessary.

3.1.2 Representation and Properties

The potential energy surface used in this work was developed by Bastiaan Braams [24, 25]. It is a global surface which allows dissociation and has a good, but not spectroscopic, quality over the whole surface. The final fit, built from 31314 *ab initio* values, has a global minimum energy of -40.44083 Hartree (1 Hartree = 2 Rydberg = 27.2107 eV) with a root mean square error of $1.4 \cdot 10^{-4}$ Hartree in the interval of $[0, 1)$ Hartree above the global minimum and still $4.02 \cdot 10^{-3}$ in the interval of $[2, 5)$ Hartree. An overview about the error distribution is given in figure 3.1.

The input for the PES is a set of mass-ordered Cartesian coordinates \mathbf{x} , the PES itself uses a set of all internuclear distances $r_{ij} = \|\mathbf{x}(i) - \mathbf{x}(j)\|$ with $r_{ij} = r_{ji}$ and $i \neq j$. If N is the number of the atoms in the molecule, there are $d = N(N - 1)/2$ internuclear distances. The potential is represented by a many body (cluster) expansion of the form

$$V_{all} = \sum_{j=0}^J \sum_{k=0}^K V_{X_j Y_k} \quad (3.5)$$

for a molecule with the totals formula $X_J Y_K$. For universality, the PES works not with molecule specific routines, but with molecule-type specific routines. For example CH_4 is of type $X_4 Y_1$, marking the mass-order, and has the cluster expansion $V = V_H + V_C + V_{H_2} + V_{HC} + V_{H_3} + V_{H_2C} + V_{H_4} + V_{H_4C}$. These potential terms are functions of the internuclear distances of the included atoms, summed over all choices which give the correct composition

$$V_{X_m Y_n} = \sum_{i_1 < \dots < i_m \in X'} \sum_{j_1 < \dots < j_n \in Y'} f_{X_m Y_n}(r_{i_1 i_2}, \dots, r_{i_{m-1} i_m}, r_{i_1 j_1}, \dots, r_{i_m j_n}, r_{j_1 j_2}, \dots, r_{j_{n-1} j_n}). \quad (3.6)$$

Let us write f as $f(\mathbf{r}) = p(\mathbf{y}(\mathbf{r})) \cdot q(\mathbf{r})$, with \mathbf{r} as the vector of the respective internuclear distances and the auxiliary variables $y(r) = \exp(-r/\lambda)$ for each component. p is a polynomial containing

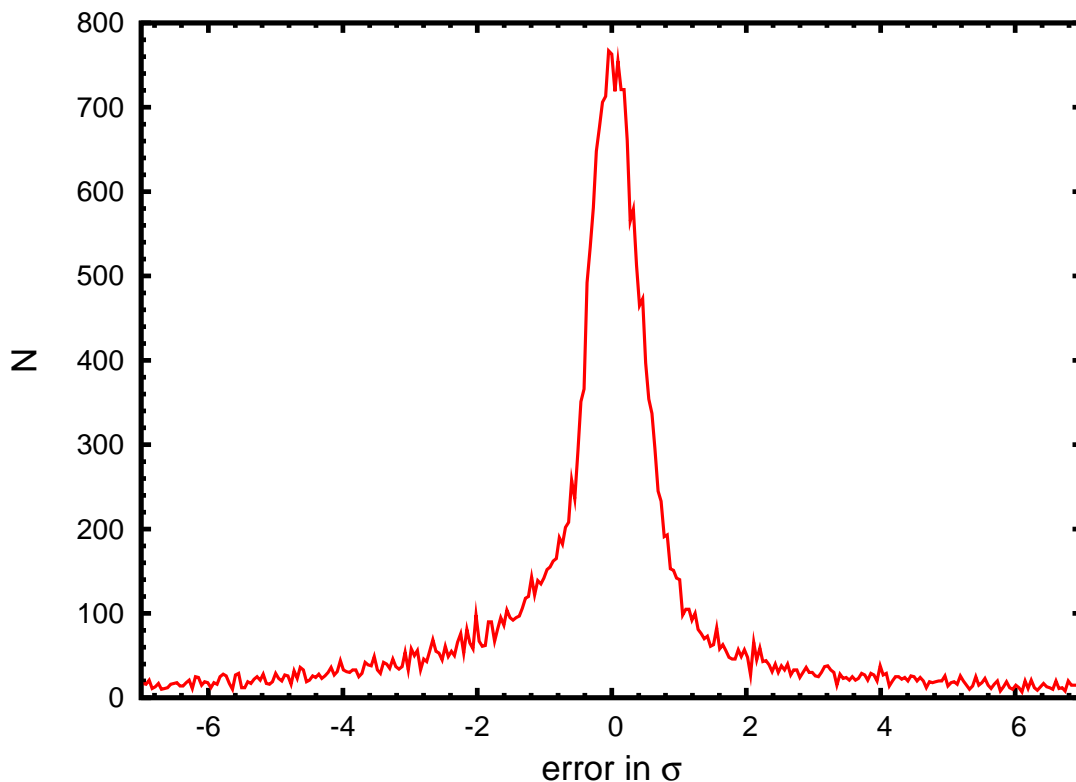


Figure 3.1: This figure shows the error distribution of the used fit. $\sigma = 4.36 \cdot 10^{-4}$ Hartree is the weighted root mean square error over all configurations.

the coefficients derived from the fitting procedure. The fit for the PES is constructed making use of the full symmetry of the molecule with invariance under the point group operations translation, rotation and reflection and the invariance under permutations of like-nuclei is conserved. The damping function $q(t(\text{rms}(\mathbf{r})))$, with $t = \text{rms}(\mathbf{r}) = \sqrt{1/n \sum (r - \bar{r})^2}$, is a function of the root mean square (rms) of the components of \mathbf{r} . For 2-body terms it is $q(t) = 1/t(\max(0, 1 - t/a))^5$ and for higher terms $q(t) = (\max(0, 1 - t/a))^5$. The one-body potentials are just the free energies of the respective atoms multiplied with their number.

The representation of the dipole moment surface is different. As discussed before, the fitted dipole moment \mathbf{d} is a vector quantity represented by

$$\mathbf{d} = \sum_i f_i(y) \mathbf{x}(i), \quad (3.7)$$

where the sum is over all atoms and $\mathbf{x}(i)$ is the vector position of the i th atom. $f_i(y)$ are polynomials that are constructed in a way, that \mathbf{d} satisfies the required permutational invariances and behaves correctly under translation. Therefore, only two of the five polynomials for methane are independent. As for the PES, the coefficients of the f_i 's are obtained by a standard least squares fitting method. The DMS has a weighted statistical error of $1.87 \cdot 10^{-3}$ Debye.

If there are m basis functions and n entries in the database, with $m \leq n$ then we have a weighted least squares system of dimension $n \times m$. For solving this problem a singular value decomposition of the associated matrix is done with the DGESVD routine of the LAPACK package [26]. The computational cost scales with $m^2 n$. For methane the computation time for the PES fit was always well below half an hour even for a basis including up to 8th order polynomials. The k th entry of the least squares system has the *ab initio* value $f(k)$. It is given a weight of $\delta/(\delta + f(k) - f_{\min})$, where f_{\min} is the lowest functional value of the database. δ is set to

0.1 Hartree as default. The problem of specifying a basis of the space of polynomials invariant under some permutational symmetry, meaning the permutation of like nuclei, is described by the theory of invariants of finite groups[27]. These invariants are obtained from the MAGMA computer algebra package [28] and are converted into Fortran Code.

3.1.3 Elements of the algorithm for the generation of spectroscopic data

1. **Construction of hypersurfaces for potential energy and dipole moments:**

Using *ab initio* data (3.1.1) a PES and DMS have to be constructed. The surface used was developed by Bastiaan Braams [24, 25].

3.2 Multimode

MULTIMODE [29, 30, 31, 32, 33, 34] is a quantum-chemical post-processing package, where post processing means calculations using a given electronic potential. In this work, the package was used to calculate rovibrational energy levels (3.2.2) of methane with the virtual configuration interaction (VCI) method (3.2.1) and corresponding transition dipole elements. It is possible to calculate exact vibrational dipole elements for $J = 0$ and approximated ones for $J > 0$. In this case the adiabatic rotation approximation (3.2.3) is used. In general the calculations are limited to one J per run and dipole elements only for $K = 0$. MULTIMODE is capable to use symmetry information up to the C_{2v} symmetry group to restrict the wave function and therefore speed-up the calculations. In contrast to an analytical potential the numerically generated PES can not guarantee perfect symmetry. Symmetry violations introduced by numerical fitting errors of the PES create additional errors like non-degeneracy of degenerate modes. Unfortunately, the usage of C_{2v} produced unsatisfying results. However, the lower symmetry C_1 overcame these problems and was used in this work. This is understandable because the reduced symmetry allows larger deviations from the ideal symmetry as always existing in numerically produced PES. The symmetry constraints used in the fitting algorithm of the PES enforces only the symmetry for the potential, but not for its derivatives.

3.2.1 Virtual Configuration Interaction

A simple method of solving the Schrödinger equation numerically is the Vibrational Self Consistent Field method (VSCF) [35, 34, 31]. In VSCF the wave function is represented as a Hartree product (2.3, 2.4), where the single modals are expanded in a primitive basis of normalmode harmonic-oscillator functions. The Schrödinger equation is solved using the variational principle. To achieve more exact solutions, virtual configuration interaction (VCI) is used [29, 36]. The many-body VCI wave function is expanded in terms of the eigenstates of a VSCF Hamiltonian, which are called virtual states. Normally the ground state Hamiltonian is used, for it can be expected to be more accurate than excited ones in most cases. The expansion forms an orthonormal basis constructing a standard eigenvalue problem. This method delivers eigenstates and -functions which are true variational upper bounds of the exact values.

MULTIMODE provides several options to construct the basis. The option used in this work is a restricted VCI basis with maximum sum quanta MAXSUM for each n-mode basis set. In addition every mode is restricted to MAXBAS quanta in the basis sets (see MULTIMODE manual [37]). The VSCF wave function assumes independent oscillators, while the vibrational modes of a molecule are coupled. A part of this coupling can be regained with the introduction of n-mode basis functions. The quality of the eigenvalues increases with a higher number of coupled modes. In theory, coupling all vibrational modes would deliver exact values. For methane 9-mode coupling would be necessary, while 5-mode coupling already exceeds the computational limits for mass production. Nevertheless, the convergence of the eigenvalues typically reaches a sufficient threshold of $\varepsilon = 1 \text{ cm}^{-1}$ for 4- or 5-mode coupling. Another factor, which influences the convergence behavior is the MAXSUM parameter. This factor determines the polynomial degree of the n-mode representations. The experience from this work shows, that this value, and also the MAXBAS value, has to be at least slightly higher than the highest vibrational mode calculated. The reason is the expansion character of the wave function. For a certain mode, all coefficients of the n-mode expansions can be non-zero. Therefore, omitting even higher excited terms changes the expansion. An infinite expansion would be exact, but normally convergence can be reached fast. Abbreviations to describe a basis with up to x mode representation and a maximum sumquanta of y is x mr y or x|y.

3.2.2 Watson-Hamiltonian

Calculations done with MULTIMODE use the Watson-Hamiltonian[38], which was introduced by Watson in 1968. It is a special form of the general molecular Hamiltonian using normal coordinates and atomic units. In atomic units the speed of light c and the Planck constant $\hbar = \frac{h}{2\pi}$ are unity. The simplification done by Watson is to resolve the general kinetic part including the determinant of the effective reciprocal inertia tensor $\mu_{\alpha\beta} = (\mathbf{I}'^{-1})_{\alpha\beta}$ into the free kinetic term and a term acting as an internal potential determined by the trace of the tensor by the use of commutation relations. This potential-like term is called Watson term and has a value of about 4 cm^{-1} for methane. The resulting Hamiltonian has the form:

$$\hat{H} = \frac{1}{2} \sum_{\alpha,\beta} \left(\hat{J}_\alpha - \hat{\pi}_\alpha \right) \mu_{\alpha\beta} \left(\hat{J}_\beta - \hat{\pi}_\beta \right) - \frac{1}{2} \sum_k \frac{\partial^2}{\partial Q_k^2} - \frac{1}{8} \sum_\alpha \mu_{\alpha\alpha} + V. \quad (3.8)$$

Greek indices represent Cartesian coordinates and Latin indices normal coordinates. The $Q_i = \sum_k l_{\alpha k, i} m_k^{1/2} (r_{\alpha k} - r_{\alpha k}^0)$ are normal coordinates, defined over the mass-scaled absolute difference of the Cartesian coordinate to the equilibrium coordinate $r_{\alpha k}^0$. \hat{J} is the total angular momentum and $\hat{\pi}$ is the vibrational angular momentum defined as

$$\hat{\pi} = -i \sum_{k,l} \zeta_{k,l}^\alpha Q_k \frac{\partial}{\partial Q_l}. \quad (3.9)$$

$\zeta_{k,l}^\alpha$ are the Coriolis coupling constants defined as

$$\zeta_{k,l}^\alpha = \epsilon_{\alpha\beta\gamma} \sum_i l_{\beta i, k} l_{\gamma i, l}. \quad (3.10)$$

The $l_{\alpha k, i}$ are constants subject to the condition that the complete matrix be orthogonal[38]. The effective moment of inertia \mathbf{I}' is the sum of the one-body inertias, corrected with the Coriolis coupling:

$$\mathbf{I}'_{\alpha\beta} = \epsilon_{\alpha\beta\gamma} \epsilon_{\beta\delta\rho} \sum_i m_i r_{\gamma i} r_{\delta i} - \sum_{k,l,m} \zeta_{k,m}^\alpha \zeta_{l,m}^\beta Q_k Q_l \quad (3.11)$$

The first term in equation 3.8 includes the rotational part of the kinetic operator. In the standard hydrogen problem this term is $\frac{l(l+1)\hbar^2}{2mr^2}$. Here the vibrational angular momentum has to be added. The second term is the translation operator along the normalmode vectors and V is the user-supplied electronic potential. MULTIMODE reads the potential values along the normalmode displacement vectors and constructs independent harmonic oscillators for each mode as a basis for the internal potential.

The potential [31] used in MULTIMODE is represented by an expansion of n -body terms with an upper limit of six coupled modes.

$$V(Q_1, Q_2, \dots, Q_N) = \sum_i V_i^{(1)}(Q_i) + \sum_{i,j} V_{ij}^{(2)}(Q_{ij}) + \sum_{i,j,k} V_{ijk}^{(3)}(Q_{ijk}) + \dots \quad (3.12)$$

In one-mode representation the oscillators are independent and

$$V^{(1)}(Q_1, Q_2, \dots, Q_N) = \sum_i V_i, \quad (3.13)$$

where only one Q_i per oscillator is non-zero. The two-mode representation is the summation over all terms with two normalmode displacements non-zero:

$$V^{(2)}(Q_1, Q_2, \dots, Q_N) = \sum_{i<j} V_{ij} - (N-2) \sum_i V_i. \quad (3.14)$$

This representation, as well as all n -mode representations with $n > 1$ contains and overcounts the representations of lower orders. Therefore, the additional term over the single-mode terms compensates for this overcounting.

This approach delivers exact rotational energies [30] with calculations scaling as J^2 , limiting the usability to small J 's. The calculation time for rovibrational energies up to $J = 35$ had an upper limit of 3 days, because for higher rotations the possible vibrational levels up to an energy limit decrease, as shown in figure 4.14.

3.2.3 Adiabatic rotation approximation

Another option to calculate rotational energies is the adiabatic rotation approximation [32], assuming a rigid rotor. Here, the $J = 0$ Watson-Hamiltonian is corrected by a simple addition of a pure rotational term.

$$\hat{H}^{AR} = \hat{H}^{J=0} + A\hat{J}_z^2 + B\hat{J}_y^2 + C\hat{J}_x^2 \quad (3.15)$$

A , B , C are the rotational constants for the respective directions. The computational costs grow linear. As shown in table 3.1 this simplification is of adequate quality for low level rotations, where the coupling between rotation and vibration is weak. The exception is the 0001 mode, where the relatively high Coriolis coupling splits the mode [29]. For higher J 's the quality decreases dramatically.

A possible improvement of the adiabatic rotation approximation would be the addition of a term linear in ζ , the Coriolis coupling constant.

$$\hat{H}^{AR+} = \hat{H}^{AR} + B\zeta[R(R+1) - J(J+1) - l(l+1)] \quad (3.16)$$

with l is the vibrational quantum number. Equation 3.16 is taken from Papoušek [39] (Chapter 20.4) and is postulated for triple degenerate states of spherical top molecules, the other states are not affected by this. A primary disadvantage is the dependency of the natural vibrational quantum numbers n_i , as these can not be obtained within MULTIMODE with limited effort. The corresponding values could be added to the final energies, but this would not improve the wave function and therefore the dipole elements.

3.2 Multimode

Table 3.1: Comparison of energies (in cm^{-1}) for exact and adiabatic rotations for fundamental excitations with $J = 1$, $J = 5$ and $J = 10$. The energies of degenerate modes split for $J > 0$ and the degeneracy is destroyed. The energies for the energetic lowest and highest fragment is printed. Every fragment includes $2J + 1$ projections, the lowest value is taken here. Adiabatic rotation does not provide the resolution of degeneracies, therefore only one value is written.

$J, n_1 n_2 n_3 n_4$	exact	adiabatic	experiment [40]
1, 0000	10.40	9.92	10.48
1, 0001	1309.31, 1323.59	1318.45	1311.4, 1326.2
1, 0100	1531.96, 1532.09	1531.48	1544.0
1, 1000	2911.89	2911.27	-
1, 0010	3012.70, 3014.42	3012.87	3028.8, 3030.5
5, 0000	156.04	133.62	-
5, 0001	1433.79, 1484.90	1441.52	-
5, 0100	1678.69, 1679.91	1658.10	-
5, 1000	3057.82	3033.09	-
5, 0010	3155.29, 3161.13	3132.38	-
10, 0000	571.13	495.82	-
10, 0001	1820.51, 1912.41	1799.74	-
10, 0100	2096.97, 2100.87	2029.37	-
10, 1000	3473.43	3389.52	-
10, 0010	3565.92, 3576.88	3482.56	-

3.2.4 Elements of the algorithm for the generation of spectroscopic data

2. Calculation of converged energies:

The energies of every rotational and vibrational state covering a user chosen interval of quantum numbers are calculated. The quantum chemical package MULTIMODE was used for this purpose.

3. Calculation of dipole matrix:

The dipole moment matrix or transition matrix is needed for the calculation of transition probabilities. MULTIMODE was used here too. The used package can calculate exact matrix elements for $J = 0$. For $J > 0$ an approximate solution (3.2.3) has to be used. $\Delta J \neq 0$ matrix elements can not be calculated.

3.3 Calculation of spectroscopic data

The further analysis is done by tools directly developed for this work. For better access several additional outputs had been added to MULTIMODE. This covers energy values with corresponding J , its projections, the leading coefficient and the vibrational quantum numbers, separated for final vibrational and final rotational states. An example output is shown in table 3.2. It was not possible to access quantum number information together with the dipole matrix elements. Instead the symmetry blocks of the left-hand (LHB) and right-hand (RHB) side are printed together with the state numbers (LHS,RHS) and the matrix elements. If the MULTIMODE calculations are done using symmetry information, the results, energies and dipoles, are grouped in blocks, corresponding to their symmetry. The energies in each block are ordered with increasing energy. Due to this, the identification of a state with this information is unique. An example output is shown in table 3.3. The processing steps of these data are described in this section, completing the algorithm at the end of the section.

Table 3.2: Part of the MULTIMODE output for a $J = 0$ 4mr8 energy calculation. K_a is the projection of the angular momentum on the z -axis and K_c is the projection on the x -axis. In addition to the quantum numbers the leading coefficient of the mode expansion is listed together with corresponding excitation numbers. The energies are relative to the ground state energy which is also given.

J	K_a	K_c	coeff.	$v_1 \dots v_9$	E [cm ⁻¹]
0	0	0	0.9980	000000000	9662.1761
0	0	0	0.7727	001000000	1308.6296
0	0	0	-0.7636	100000000	1308.6638
0	0	0	-0.6383	010000000	1308.7137
0	0	0	-0.9951	000010000	1521.4429
0	0	0	0.9951	000100000	1521.4652
0	0	0	0.5543	002000000	2583.6712
0	0	0	-0.7411	002000000	2609.9436
0	0	0	0.6217	020000000	2610.5633
0	0	0	-0.7858	110000000	2611.4266
0	0	0	-0.5246	101000000	2620.7172
0	0	0	-0.7374	101000000	2621.2509
⋮	⋮	⋮	⋮	⋮	⋮
0	0	0	0.2888	010100100	5813.3575
0	0	0	0.3493	001010010	5814.7976
⋮	⋮	⋮	⋮	⋮	⋮

3.3.1 State analysis

MULTIMODE uses the complete set of vibrational modes independent of possible degeneracies. Therefore, a routine has to be added to transform the v_i 's into n_i 's through adding up the quantum numbers of the corresponding v_i . Examples can be taken from tables 3.2 and 3.4. Methane has one non-degenerated and three degenerated vibrational modes. To obtain the reduced state information it is appropriate to add up the excitation values for the parts of the

3.3 Calculation of spectroscopic data

Table 3.3: Part of the MULTIMODE output for a $J = 0$ 4mr8 dipole calculation. LHB and RHB are the symmetry block numbers for the left-hand and right-hand state, while LHS and RHS are the numbers of the states in the blocks.

LHB	LHS	RHB	RHS	M_{ij} [atomic units]
1	1	1	1	0.269670D-06
1	1	1	2	0.198040D-01
1	1	1	3	-0.103576D-01
1	1	1	4	0.919631D-02
1	1	1	5	0.351034D-05
1	1	1	6	0.153437D-06
1	1	1	7	0.795802D-06
1	1	1	8	0.950961D-03
1	1	1	9	-0.142610D-02
1	1	1	10	0.114832D-02

degenerated mode leading to the following rule:

$$n_1 = v_6 \quad (3.17)$$

$$n_2 = v_4 + v_5 \quad (3.18)$$

$$n_3 = v_7 + v_8 + v_9 \quad (3.19)$$

$$n_4 = v_1 + v_2 + v_3 \quad (3.20)$$

The $n_4 = 2$ overtone for example can be built from $\frac{(2+3-1)!}{2!(3-1)!} = 6$ different configurations. As shown in figure 3.2, there are six different states calculated, but the v_i 's are not distributed as expected. Some configurations are doubled, some are missing. This leads to a complex problem involved with VCI theory and the used potential representation.

The assignment of the vibrational quantum numbers is naturally done by searching for the largest coefficient of the state expansion. For a pure basis the fundamental excitations would have leading coefficients near one, as for lines 1,5,6 in table 3.2. This is not true, if one looks for higher excitations, as in the last two lines of table 3.2. As can be seen in this example, the assignment of quantum numbers is not necessarily correct.

Still for higher excitations and higher rotational quanta the leading coefficients are of similar values, typically between 0.2 and 0.4, which can be seen in table 3.2 in the last two lines. The quantum numbers assigned can not be considered as reliable and may lead to wrong physical quantum numbers. Calculations were done to test the appearance of wrong assignments. For $J = 0$ only few states have wrong assignments. If this shortcoming would be conserved for $J > 0$ a list of states to be corrected and their true quantum numbers could be made by hand and it can be used to automatically adjust the $J > 0$ assignments. Unfortunately, this effect grows with raising J , producing more and more unreliable assignments for high J s. In addition the K projection assignments appeared to be affected by the same problem, for the number of states per K was not equal, although before the final rotational VCI step they were and no states vanished. The described problem can be minimized with an improvement of the PES, but it can not be finally resolved for it is an intrinsic property of the state expansion.

For higher excitations degenerated modes split into sub-bands. The already discussed $n_4 = 2$ example would have an energy of $E_{n_4=2} = 2 \cdot E_{n_4} \approx 2619 \text{ cm}^{-1}$ without coupling. For the used level of theory, 4mr8, the band splits into three sub-bands, A_1, F_2, E , from 2583.7 cm^{-1} to 2621.3 cm^{-1} as can be seen from table 3.4. The sub-bands and their symmetries are given by group theory [17], but not the energy ordering of the sub-bands which have to be determined

Table 3.4: Intermediate post processing step of output shown in table 3.2. The left most column is a counter for the states of one J value.

count	J	K_a	K_c	$n_1 \dots n_4$	E [cm ⁻¹]
1	0	0	0	0000	0.0000
2	0	0	0	0001	1308.6296
3	0	0	0	0001	1308.6638
4	0	0	0	0001	1308.7137
5	0	0	0	0100	1521.4429
6	0	0	0	0100	1521.4652
7	0	0	0	0002	2583.6712
8	0	0	0	0002	2609.9436
9	0	0	0	0002	2610.5633
10	0	0	0	0002	2611.4266
11	0	0	0	0002	2620.7172
12	0	0	0	0002	2621.2509
⋮	⋮	⋮	⋮	⋮	⋮
20	10	6	5	0000	571.3743
21	10	7	3	0000	571.3746
22	10	7	3	0001	1820.5116
23	10	6	4	0001	1820.6182
⋮	⋮	⋮	⋮	⋮	⋮

by experiment. For a physical correct analysis this symmetry splitting should be taken into account while processing the data. The examined energy interval experiments [10] deliver data for comparison and also information about the splitting. This would allow a mapping of states into sub-bands, but to apply this information, correct quantum number assignments would be necessary.

Since there is no way to assign the sub-bands correctly to the states, one single energy has to be used for all states with the same vibrational quantum numbers. This average energy is a good approximation, because effects of wrong assignments are averaged out under the assumption that the number of wrong assigned cases is small compared to the degeneracy of a given band. The standard deviation is the proper quantity to estimate the quality of this assumption and is therefore included in the final energy file. A part of this file is printed in table 3.5. For most states the deviation is of the same order as the typical uncertainty, of the order of a few percent due to the accuracy of the PES. The exception are excitations of the n_4 mode which split strongly due to the Coriolis coupling, as discussed before. The effect can be seen in table 3.4 represented by the large mode splitting and in table 3.5 as a larger standard deviation for bands with n_4 content. The degeneracy factors g for further analysis are calculated by theoretical considerations, not by counting. The assigned quantum numbers are not absolutely reliable, as mentioned before. The total numbers of states occurring for one band can differ from the true value due to this. The correct number is given by permutations, the number of possibilities to allocate a number of excitations n to a number of modes m :

$$g = \frac{(n + m - 1)!}{n!(m - 1)!} \quad (3.21)$$

The obtained energies are of appropriate accuracy for most cases, as can be seen from the standard deviations in table 3.5. The energy information can be used for the following steps.

3.3 Calculation of spectroscopic data

Table 3.5: Part of the final energy list. In addition to the average energy of each band the standard deviation σ of this value is given together with the degeneracy factor g .

J	K_a	K_c	$n_1 \dots n_4$	E [cm ⁻¹]	σ [cm ⁻¹]	g
0	0	0	0000	0.0000	0.0000	1
0	0	0	0001	1308.6690	0.0345	3
0	0	0	0002	2609.5955	12.4901	6
0	0	0	0003	3905.5788	27.5704	10
0	0	0	0004	5195.6609	42.8934	15
0	0	0	0010	3003.5315	0.1821	3
0	0	0	0011	4305.7781	2.2459	9
0	0	0	0012	5607.5294	18.0929	18
0	0	0	0020	5992.9241	20.0145	6
0	0	0	0100	1521.4541	0.0112	2
0	0	0	0101	2826.4448	7.8680	6
0	0	0	0102	4134.6408	25.5492	12
0	0	0	0103	5432.1794	39.5879	20
0	0	0	0110	4515.9985	3.3828	6
0	0	0	0111	5829.8221	10.2947	18
⋮	⋮	⋮	⋮	⋮	⋮	⋮

3.3.2 Dipole moment matrix

As described above, MULTIMODE is capable of calculating exact matrix transition elements for $J = 0$ and approximated ones for $J > 0$, but only for $K = 0$. Data for $\Delta J \neq 0$ and $\Delta K \neq 0$ can not be obtained. The output for the dipole elements does not include any quantum number information, but the elements are ordered in the same way as the corresponding states. The MULTIMODE output is given in table 3.3. So state information can be recovered by comparison with the energy output file. For this purpose the complete energy output is read into memory in form of table 3.4, therefore the counting in the first column. Each line of the dipole data is taken and the corresponding states for the left-hand and right-hand sides are looked up in the list of energy states. The output, as printed in table 3.6, then contains the quantum number

Table 3.6: Intermediate processing step of output shown in table 3.3. For each dipole element the rotational quantum number and the vibrational quantum numbers of the left-hand (LH) and right-hand (RH) side are given.

J	n_{LH}	n_{RH}	M_{ij} [atomic units]
0	0000	0000	0.269670E-06
0	0000	0001	0.198040E-01
0	0000	0001	-0.103576E-01
0	0000	0001	0.919631E-02
0	0000	0100	0.351034E-05
0	0000	0100	0.153437E-06
0	0000	0002	0.795802E-06
0	0000	0002	0.950961E-03
0	0000	0002	-0.142610E-02
0	0000	0002	0.114832E-02
⋮	⋮	⋮	⋮

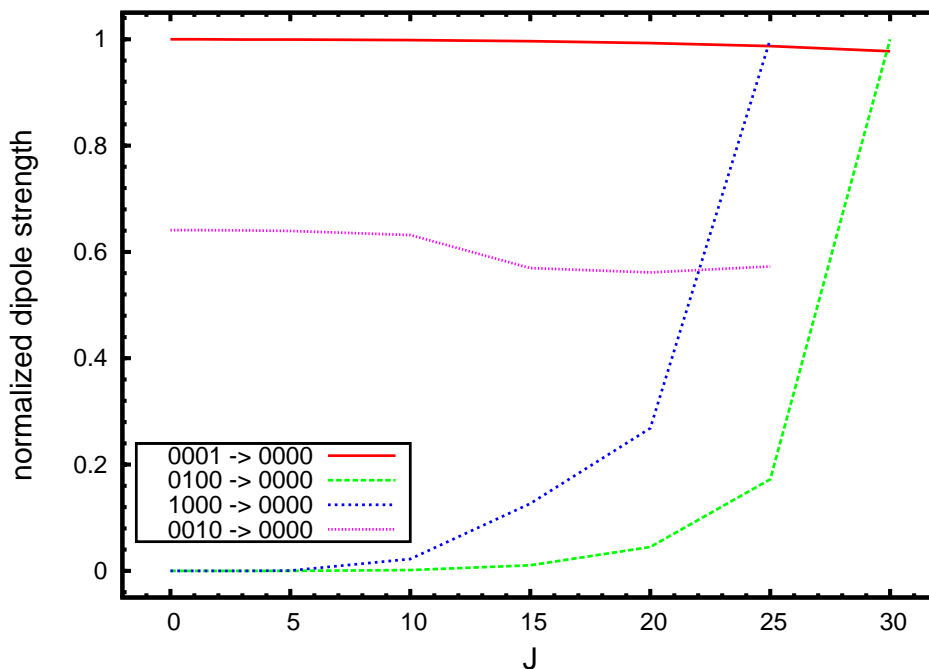


Figure 3.2: The dependency of the squared dipole elements on J is shown. The values are normalized, the factors are $0.1947 \cdot 10^{-03}$ for $0001 \rightarrow 0000$, $0.5806 \cdot 10^{-06}$ for $0100 \rightarrow 0000$, $0.1366 \cdot 10^{-04}$ for $1000 \rightarrow 0000$ and $0.1947 \cdot 10^{-03}$ for $0010 \rightarrow 0000$. It can be seen, that for low rotations only the triple degenerated modes are infrared active, in agreement with theory and experiments.

information of the upper and lower level for each element. For $J = 0$ the matrix elements are calculated from the same wave functions used for the energy calculations. Therefore, a correct one-to-one assignment can be done, allowing the construction of spectroscopic information for each possible single line. For $J > 0$ the energy values are calculated with the exact rotational Hamiltonian, while the dipole elements are obtained using the adiabatic rotation approximation (3.2.3). This does not allow a direct mapping between energies and dipoles.

Hence, the calculations for dipole elements are expensive and the dependence of the elements on J is smooth (see figure 3.2), calculating these elements for certain J s and then interpolating linearly in between is a practical approach. The vibrational infrared active modes are independent from rotation, whereas for the infrared inactive modes the dependency is quadratic in J , reaching a noticeable dipole strength for higher J . Since no information is available for the K -dependency, the elements are assumed to be independent. For $\Delta J \neq 0$ transitions the matrix element is assumed to be the average of the corresponding elements for both J s.

The natural way of calculating the matrix elements, would be the direct calculation of the scalar product of the dipole operator with the wavefunction. This is not possible at the moment, because MULTIMODE do not provide an interface to get the wave function externally available nor does the author, Stuart Carter, support help or changes to the code. There is no other method available than the one used. A time-consuming rewriting of the code to achieve the wave function information and to calculate any dipole matrix element has to be done. This is complicated by the Fortran 77 code structure and non-standard coding. The work is assumed to need approximately one year of time with the collaboration of the author. This is beyond the scope of a diploma thesis and is planned to be done within a PhD thesis instead. Nevertheless, this work is a first step, which achieves sufficient accuracy for the astrophysics and which can

be used as a benchmark for the further development as well.

The exact mapping of the dipole elements to quantum numbers is not possible due to the uncertainty in the reliability of the quantum number information, as discussed for the energy evaluation before (3.3.1). Again, the only viable way is to average out the dipole elements for each transition with identical quantum numbers. In contrast to the energies, this is a less satisfying approach. The dipole strength for the same transition, but with different sub-bands involved may vary over several orders of magnitude. This is visibly pronounced for the 0000 \rightarrow 0002 translations in table 3.6. An averaging is not affecting quality, as long as all the translations are assigned to their correct corresponding bands. If this is not the case, the effective dipole strength may deviate strongly from the value, obtained with correct assignment. A quality estimation of this approximation can not be given, nor can it be given for the adiabatic rotation matrix elements themselves. The only check will be done by comparing the final results with existing spectroscopic data.

Calculations of dipole matrix elements were done for $J = 0, 1, 3, 5, 10, 15, 20, 25, 30$. The list of dipole elements as printed in table 3.6 were taken and the average of the squared transition elements were calculated. Using this list, a linear interpolation of the average squared dipole elements as a function of J was done. Afterwards, the complete list of all dipole matrix elements for all J s was saved, a part of it is shown in table 3.7.

Table 3.7: Intermediate processing step of output shown in table 3.3. For each dipole element the rotational quantum number and the vibrational quantum numbers of the left-hand (LH) and right-hand (RH) side are given.

n_{LH}	n_{RH}	M_{ij}^2 [atomic units]					
		$J = 0$	1	2	3	4	5
0000	0000	0.7083E-12	0.1174E-10	0.1049E-09	0.1980E-09	0.1776E-08	0.3354E-08
0000	0001	0.1947E-03	0.1947E-03	0.1947E-03	0.1946E-03	0.1946E-03	0.1946E-03
0000	0100	0.6996E-11	0.4114E-11	0.9548E-11	0.1498E-10	0.3567E-10	0.5637E-10
0000	0002	0.7133E-06	0.7130E-06	0.7129E-06	0.7127E-06	0.7126E-06	0.7124E-06
0000	0101	0.1834E-05	0.1833E-05	0.1833E-05	0.1833E-05	0.1835E-05	0.1838E-05
0000	1000	0.8227E-10	0.4463E-10	0.2978E-09	0.5509E-09	0.4011E-08	0.7471E-08
0000	0010	0.1248E-03	0.1248E-03	0.1247E-03	0.1247E-03	0.1246E-03	0.1245E-03
0000	0200	0.3794E-10	0.8742E-10	0.1185E-09	0.1495E-09	0.2641E-08	0.5132E-08
0000	0003	0.1016E-06	0.1016E-06	0.1019E-06	0.1021E-06	0.1025E-06	0.1030E-06
0000	0102	0.5555E-07	0.5547E-07	0.5541E-07	0.5535E-07	0.5515E-07	0.5494E-07
0000	1001	0.2349E-05	0.2349E-05	0.2346E-05	0.2342E-05	0.2335E-05	0.2328E-05
\vdots	\vdots	\vdots	\vdots	\vdots	\vdots	\vdots	\vdots

3.3.3 Einstein coefficients

The final data given to astrophysics are spontaneous emission probabilities A_{ij} per second per molecule, called Einstein coefficients [41]. These probabilities have a cubic dependency on the wavenumber of the electromagnetic wave sent out and on the absolute square of the transition dipole elements M_{ij} .

$$A_{ij} = \frac{16\pi^3}{3h^4c^3} \frac{(E_i - E_j)^3}{2J_i + 1} |M_{ij}|^2 \quad (3.22)$$

i and j are the indices of the two rovibrational states involved. $2J_i + 1$ is the g_J -factor of the upper state. The wavenumber of a given transition is the energy difference between the involved states divided by the Planck constant and speed of light: $k = \frac{\Delta E}{hc} = \frac{2\pi\Delta E}{hc}$. For calculating

Table 3.8: Hönl-London Rotational Line Strength Factors [45]

S_{JK}	$\Delta K = +1$	$\Delta K = 0$	$\Delta K = -1$
$\Delta J = +1$	$\frac{(J_j+2+K_j)(J_j+1+K_j)}{4(J_j+1)}$	$\frac{(J_j+1+K_j)(J_j+1-K_j)}{(J_j+1)}$	$\frac{(J_j+2-K_j)(J_j+1-K_j)}{4(J_j+1)}$
$\Delta J = 0$	$\frac{(J_j+1+K_j)(J_j-K_j)(2J_j+1)}{4J_j(J_j+1)}$	$\frac{(2J_j+1)(K_j)^2}{J_j(J_j+1)}$	$\frac{(J_j+1-K_j)(J_j+K_j)(2J_j+1)}{4J_j(J_j+1)}$
$\Delta J = -1$	$\frac{(J_j-1-K_j)(J_j-K_j)}{4J_j}$	$\frac{(J_j+K_j)(J_j-K_j)}{J_j}$	$\frac{(J_j-1+K_j)(J_j+K_j)}{4J_j}$

the transition dipole elements M_{ij} the vibrational ones from MULTIMODE are used in this work. The $J > 0$ elements only account for the vibrational part of these states. For only vibrational transition elements $M_{v_i v_j}$ are available for this work, an additional approximation has to be done by substituting the M_{ij} with Hönl-London factors $S_{J_j K_j}$ [42, 43, 44]

$$|M_{ij}|^2 = S_{J_j K_j} |M_{v_i v_j}|^2 \quad (3.23)$$

The Hönl-London factors, listed in table 3.8, are meant to take into account the rotational dependence of vibrational bands. The basic idea of Hönl and London [44] was to obtain the intensity relations between the different branches of rotational lines. They used the correspondence principle to obtain the intensity ratios in terms of the angle $\cos \Theta = \frac{K}{J}$ between the angular momentum and its projection. Using similarities between the molecular and the atomic problem, the intensity splitting for the branches is considered to be equivalent to the Zeeman effect. The relations they provide differ partly from modern tables. A paper published in 2005 by Hansson and Watson [41] discussed irregularities within the literature about the exact formulas for this factors and derived them for the special case of diatomic molecules.

The Hönl-London factors modify the relative intensities of rotational lines according to the algebra of quantum mechanics. If one assumes the rotational and vibrational parts of the wavefunction to be independent one may separate the transition problem into vibrational and rotational part, as Cantarella did in 1992 [46]. The Hönl-London factors do not account for this. Therefore, equation 3.23 does not account for rotational driven transition probabilities at all, besides the level included in the adiabatic rotation approximation. Still, the ansatz at least ensures the branch splitting according to the theory. This is an approximation with unknown quality. Although dipole matrix elements are calculated for several J s, the matrix elements are pure vibrational and therefore do not replace the Hönl-London factors.

Substituting equation 3.23 in equation 3.22 and multiplying with the g factors for lower and higher state, the final Einstein coefficients are obtained:

$$A_{ij} = \frac{16\pi^3}{3h^4 c^3} \frac{(E_i - E_j)^3}{2J_i + 1} g_i g_j S_{J_j K_j} |M_{v_i v_j}|^2 \quad (3.24)$$

3.3.4 Elements of the algorithm for spectroscopic data

4. Interpolation of dipole matrix:

Instead of calculating the dipole matrix for every J , every fifth J dipole matrices are calculated and then interpolated.

5. Calculation of Einstein coefficients:

Using the dipole matrix elements the transition probability for every possible transition is calculated. With this information intensity spectra can be obtained.

3.4 Summary of the algorithm

The algorithm shown here satisfies the requirements discussed before. It is general, meaning it can be used for any kind of hydrocarbons, not only methane. It can be easily adapted or modified for other purposes. Clearly, the scope of a diploma thesis defines further practical limits for improvements and extensions of the algorithm.

1. Construction of hypersurfaces for potential energy and dipole moments:

Using *ab initio* data (3.1.1) a PES and DMS have to be constructed. The surface used was developed by Bastiaan Braams [24, 25] (3.1.2).

2. Calculation of converged energies:

The energies of every rotational and vibrational state covering a user chosen interval of quantum numbers are calculated. The quantum chemical package MULTIMODE (3.2) was used for this purpose.

3. Calculation of dipole matrix:

The dipole moment matrix or transition matrix is needed for the calculation of transition probabilities. MULTIMODE was used here too. The used package can calculate exact matrix elements for $J = 0$. For $J > 0$ an approximate solution (3.2.3) has to be used. $\Delta J \neq 0$ matrix elements can not be calculated.

4. Interpolation of dipole matrix:

Instead of calculating the dipole matrix for every J , every fifth J dipole matrices are calculated and then interpolated.

5. Calculation of Einstein coefficients:

Using the dipole matrix elements the transition probability for every possible transition is calculated. With this information intensity spectra can be obtained.

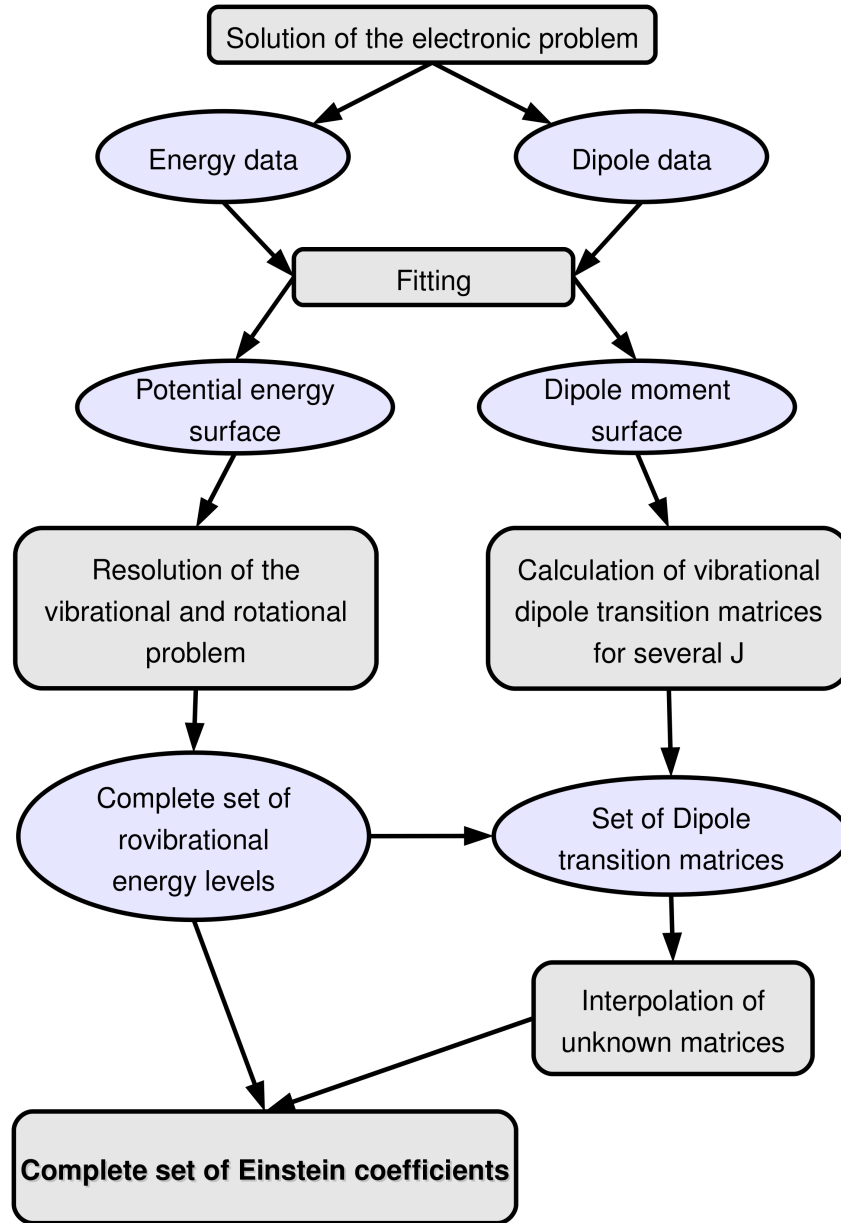


Figure 3.3: Flowchart of the algorithm to obtain spectroscopic data.

As a conclusion for the conceptual part of this work it can be said, that many approximations had to be made to have the possibility of getting spectroscopic data. Nevertheless, the quality of the coefficients is expected to be sufficient for astrophysical applications. Deviations of the energies from experimental results have no strong impact on the Einstein coefficients, because they have a cubic dependence on transition energies. Errors in the energies of about some percents (already given by the PES) do not affect the Einstein coefficients strongly due to the cubic dependence. Also, wavenumber differences of some percents are uncritical, because the astrophysical observations have large errors in comparison. The quality of the dipole matrix elements is unknown for all except the $J = 0$ case. Whether the approximations, which had to be done are reliable can be seen only by a comparison of the data from other databases. This is presented in chapter 4.

Chapter 4

Results

In this chapter the results are presented, beginning with tests of the PES and the vibrational calculations. The final Einstein coefficients are calculated and analysed. The quality of the coefficients is tested by constructing several intensity spectra. These tests include the comparison with the HITRAN database. Finally, an example for an astrophysical application of the provided data is given.

4.1 Tests

4.1.1 PES properties

The MULTIMODE program package which is used to calculate rovibrational energies is working with normalmode coordinates q_i . Therefore, a good visual test of the quality of the PES is to compare one-dimensional cuts along the vectors of normalmode displacements through the PES with *ab initio* values. This is done for all degenerated modes. In figure 4.1 the threefold degenerated modes v_1 to v_3 are shown. In this figure, the potential value of a configuration is plotted against the corresponding normal mode displacement.

The PES values of modes v_1 and v_3 show very good agreement, while mode v_2 deviates from the other two and from the *ab initio* values. This can be seen better in figure 4.3 where the second derivatives of the potentials are displayed. Hence the potentials are still similar, the orthogonal normalmode vectors are represented with only minor deviations. The potential for these modes should be strictly symmetric, which it is not the case here. But the deviation from the symmetric shape is relatively small, especially for small oscillations. The comparison with the *ab initio* values for v_1 shows a very good agreement with the PES.

In the same figure the PES values for the twofold degenerated modes v_4 and v_5 are plotted together with *ab initio* values for v_4 . v_5 has an asymmetric potential as expected from symmetry. The v_4 normalmode vector agrees quite well with the *ab initio* calculations. Degeneracy of these modes will be destroyed for higher excitations, where the deviations of the PES between the two modes get larger.

The same analysis has been done for the other vibrational modes and is shown in figure 4.2. Mode v_6 is singular. The PES representation of the potential is good for $q > -1$. For $q < -1$ the PES does not represent the *ab initio* calculated values. The modes v_7 to v_9 are asymmetric stretch modes which are represented by symmetric potentials. This is in agreement with the *ab initio* data. The corresponding PES representation of v_7 is also symmetric but it shows larger deviations from the *ab initio* data. The other two modes are tilted but show a similar shape, if the potentials are rotated.

The direct comparison between *ab initio* data and corresponding PES values in cuts along the different normalmode vectors reveals deviations. These deviations are more pronounced for the higher energy modes. This test does not directly predict the quality of the following MULTIMODE calculations, but it demonstrates possibilities for improvements of the PES. This is especially true, because even if the eigenvalues of the methane wave function might be in the order expected by the root mean square error of the PES, the composition of the wave function in terms of the harmonic excitations might be mixed up for the oscillators having wrong normalmode

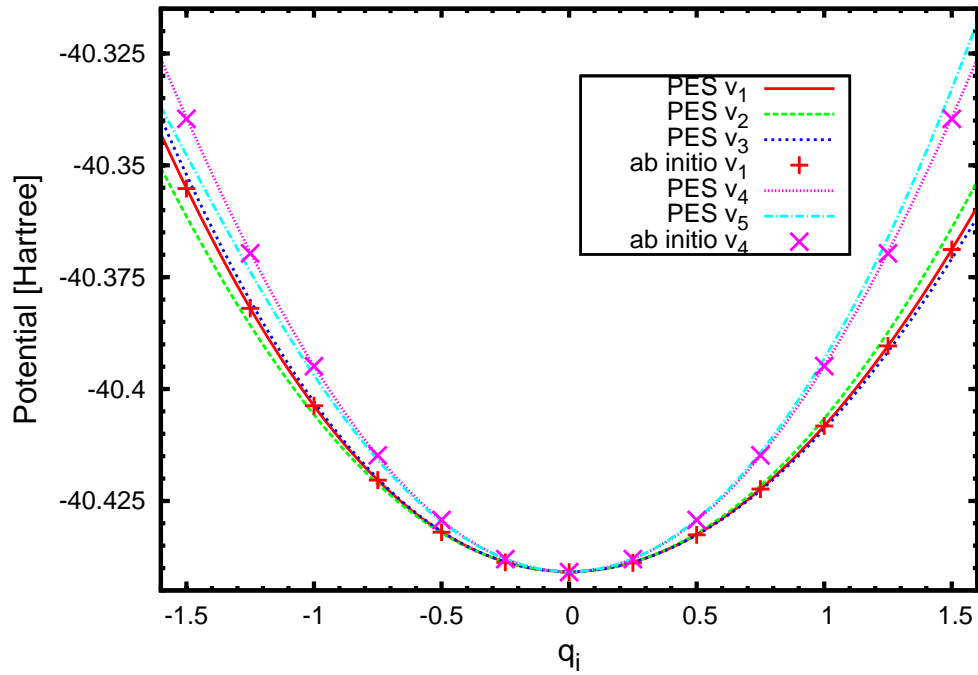


Figure 4.1: This figure shows the PES representations of threefold degenerated modes v_1 - v_3 and the twofold degenerated modes v_4 , v_5 . In addition the *ab initio* potential values of v_1 and v_4 are shown for comparison. The q_i 's are factors of the respective mass-scaled normalmode vectors (normalmode displacements).

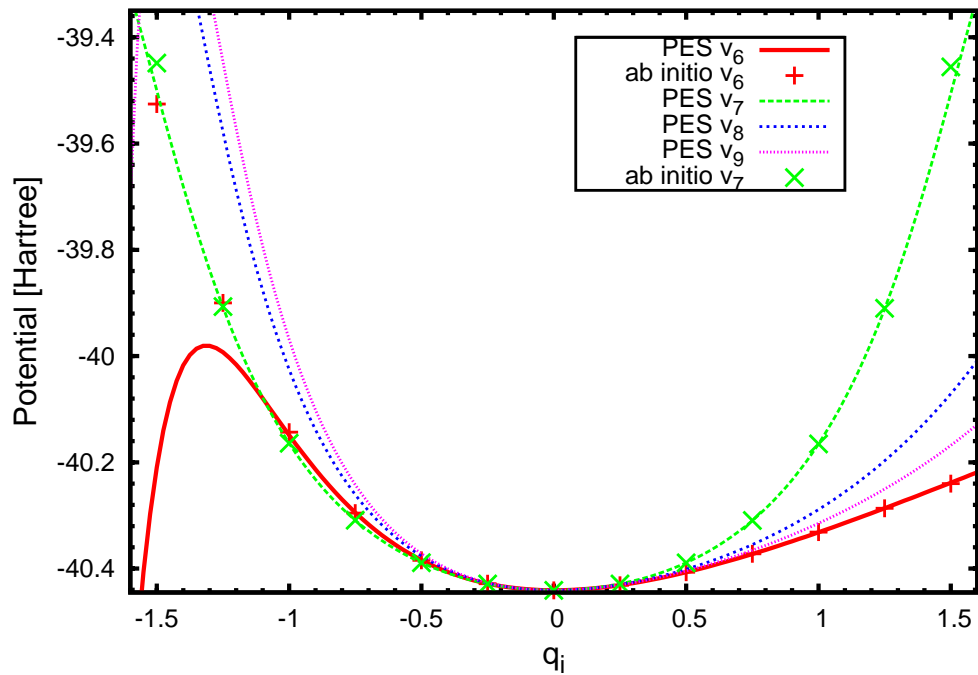
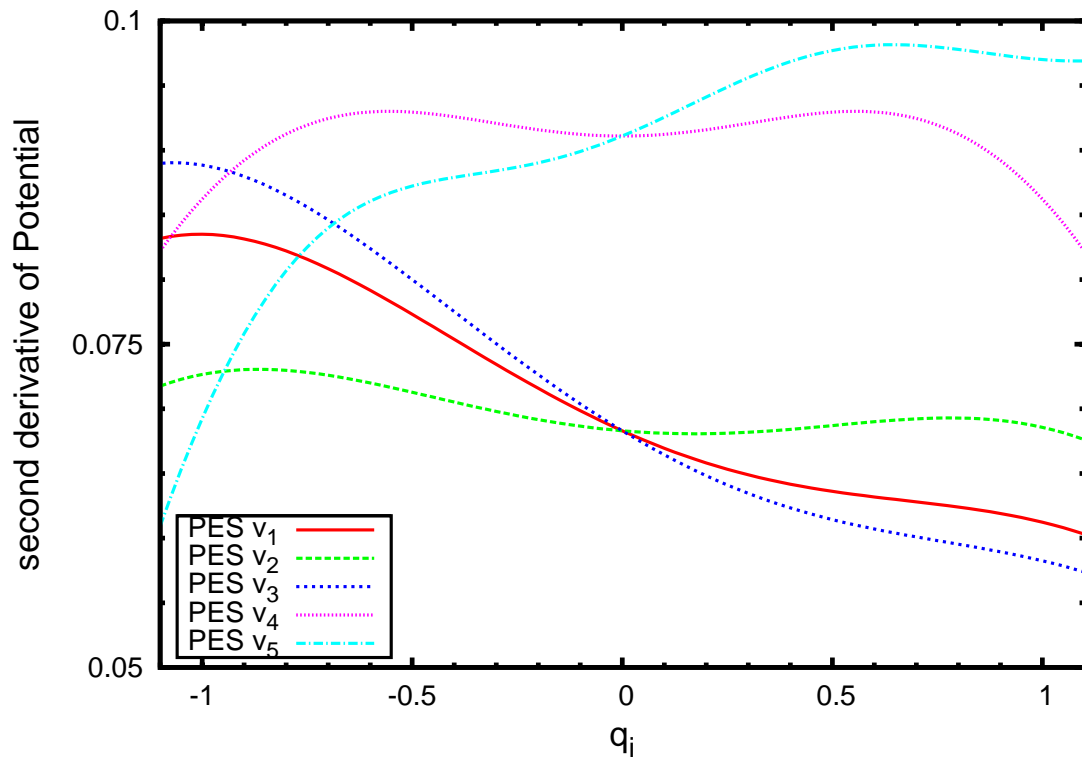
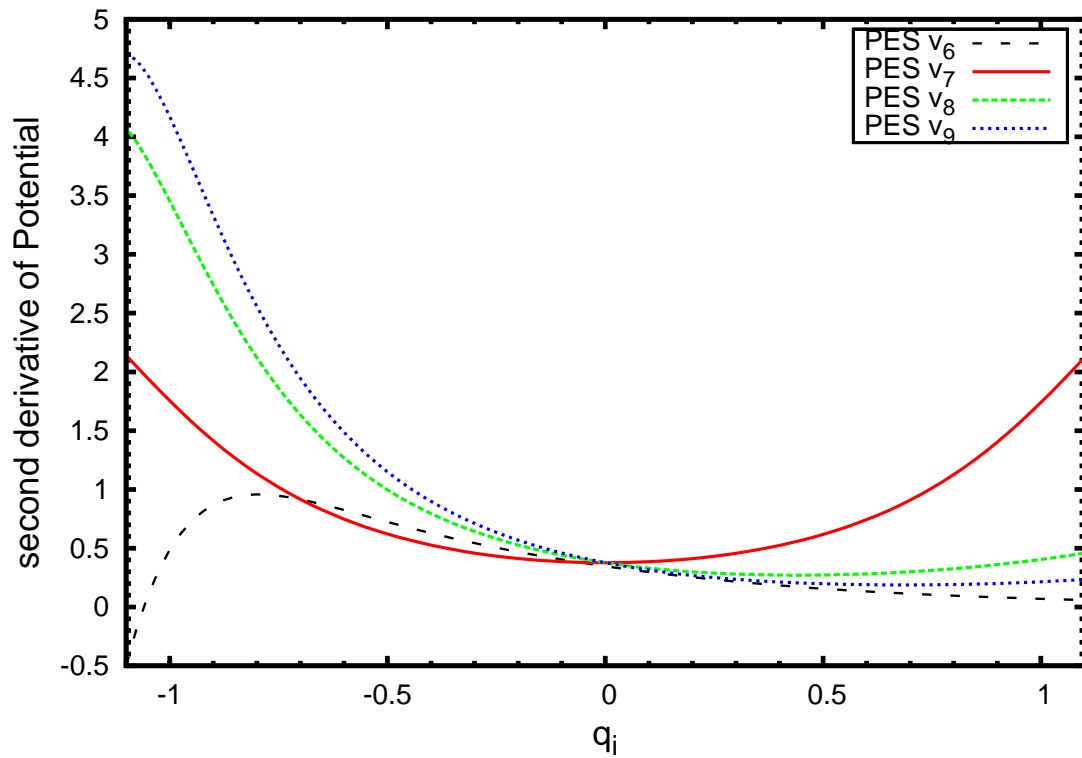


Figure 4.2: Similar to figure 4.1 this figure shows the PES representations of non degenerated mode v_6 and the threefold degenerate modes v_7 - v_9 . For comparison the *ab initio* values of v_6 and v_7 are included.

Figure 4.3: Figure of the second derivatives of potential for v_1 to v_5 .Figure 4.4: Figure of the second derivatives of potential for v_6 to v_9 .

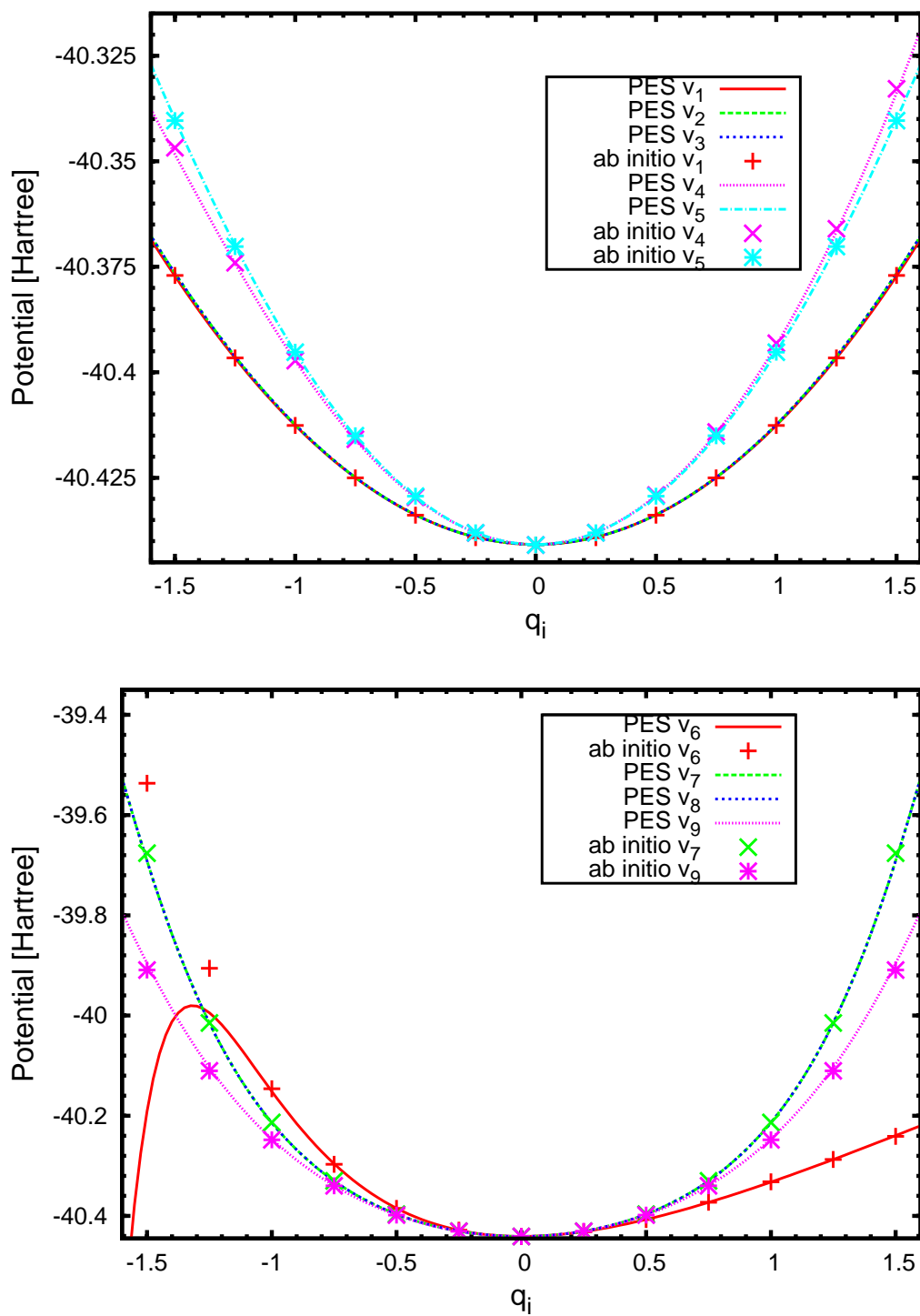


Figure 4.5: Comparisons of PES and *ab initio* MOLPRO data under the usage of MOLPRO calculated normalmode vectors.

orientations. Therefore, additional fine-tuning of the PES is needed, especially trying to enforce strictly all symmetry constraints. Up to now this is done implicitly only for the potential itself, but not for its derivatives.

An additional test was done with normalmode vectors calculated with MOLPRO for the PES global minimum. The results are plotted in figure 4.5. For these vectors the PES is fitting well the *ab initio* data with the exception of mode v_6 . It is the only mode with identical normalmode vectors for both methods, as without degeneration there are no degrees of freedom available. The reason for the irregularity of the PES regression may be badly converged *ab initio* data. These can exist, especially for strongly stretched or twisted molecules, where already multi-reference calculations will be necessary. Also, the PES fit can have problems. The PES fit was done not only with CH_4 data but also with data of fragments like $\text{CH}_3 + \text{H}$. This is the characteristics of a global PES. Discontinuities in the original data dominated by two different fragment types can cause such problems. Although the energy of the PES and from *ab initio* data show in general quite satisfying agreement, the curves of the energies in the directions of specific normalmodes do not in every case, e.g. modes v_4 and v_5 do not match. The first three modes have energy levels which are overall too low, as the last three have. Even though these normalmode vectors are delivering mostly the expected symmetric potentials, the usage for MULTIMODE calculations failed. These vectors deliver much too low energies, lower than 10% as is shown in table 4.1.

From this analysis it is concluded that the construction of an improved PES should be done if higher accuracies are needed. The quality of the PES itself is sufficient for this work with an approximated error of 30 cm^{-1} , as discussed in chapter 3. The deficiencies of the normalmode vectors lead to smaller CI coefficients and more mixed states. This has no major influence on the energy values, but on the associated quantum numbers. In addition the dipole matrices suffer due to changed symmetries. An improvement can be achieved by adding more data points near the global minimum, to give the local area near the global minimum of the PES a higher weighting. The other observation is, that the normalmode vectors are critical and can also be further improved by improving the PES as discussed before. If the PES represents the *ab initio* data well for all modes, the normalmode vectors should get close to the exact MOLPRO normalmode displacements.

During this work several computers were used for calculations. Deviations larger than machine precision between identical calculations on different machine occurred, demonstrating the need for an improved conditioning of the final matrix solved for the PES fit.

Table 4.1: The converged CI energies of the fundamental excitations are shown under the usage of MOLPRO calculated normalmode vectors. Although the leading coefficients are all larger than 0.9 and are therefore better than the ones used in this work (compare table 3.2) the energies are far too small.

coeff.	$v_1 \dots v_9$	$E [\text{cm}^{-1}]$
0.9918	000000000	9116.4631
0.9749	001000000	1137.5199
0.9749	010000000	1137.5200
0.9769	100000000	1137.7601
-0.9911	000010000	1520.1673
-0.9911	000100000	1520.2251
0.9348	000000100	2828.1546
0.9348	000000010	2828.1546
0.9401	000000001	2828.5141
0.9712	000001000	2883.5740

4.1.2 Harmonic oscillator

The most primitive potential able to describe a vibrational movement is the harmonic oscillator (HO) potential as discussed in 2.2.4. MULTIMODE uses an harmonic oscillator approximation for the potentials of the normalmodes to built up its n -body expansions of the potential. This low order approach allows a fast, rough estimate of the expected energy values and more important the range where the potential is really used.

Figures 4.6 and 4.7 show the harmonic oscillator potentials and their energy levels. For a better comparison the PES values are plotted as points into the figures. This shows, that the HO is a realistic approximation at least for some modes, v_1 and v_4 . The strongly asymmetric mode v_6 can not be represented by a harmonic oscillator, but still an appropriate energy expectation is delivered. Table 4.2 shows the HO energies of the fundamentals together with the CI energies and experimental data. It can be seen that the HO approximation delivers true upper limits for the energies with no more than 5% overestimation in this case. The lower modes, which had a nearly harmonic shape, reach a lower overestimation. Especially mode v_4 , where no major deviations between HO and PES are obvious, reaches an overestimation of only 1.2% which is almost as good as the CI underestimation of 0.77%.

The harmonic oscillator approximation is therefore an appropriate first order approximation for molecular vibrational energies. The results suggests a fair quality of the MULTIMODE calculations despite the problems with the normalmode vectors.

Table 4.2: Comparison of harmonic oscillator (HO) energies with CI energies and experimental data [10].

E_{HO} [cm^{-1}]	E_{CI} [cm^{-1}]	E_{Exp} [cm^{-1}]
1343.33	1308.62	1310,8
1343.45	1308.66	1310,8
1343.45	1308.71	1310,8
1551.44	1521.44	1533,3
1551.53	1521.46	1533,3
3028.86	2901.45	2916,5
3156.29	3003.27	3019,6
3156.29	3003.65	3019,6
3156.30	3003.66	3019,6

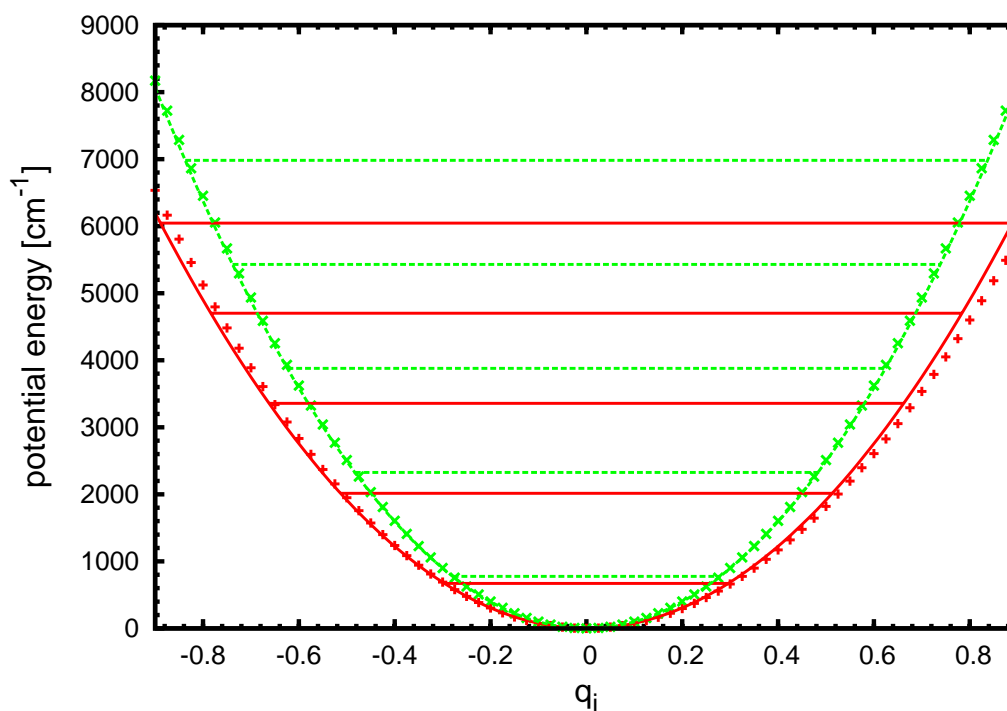


Figure 4.6: Plot of the approximated harmonic potential (lines) and harmonic oscillator levels for v_1 (red) and v_4 (green). The corresponding PES values are plotted as points. The harmonic representation of these modes is adequate, the modes are of harmonic nature.

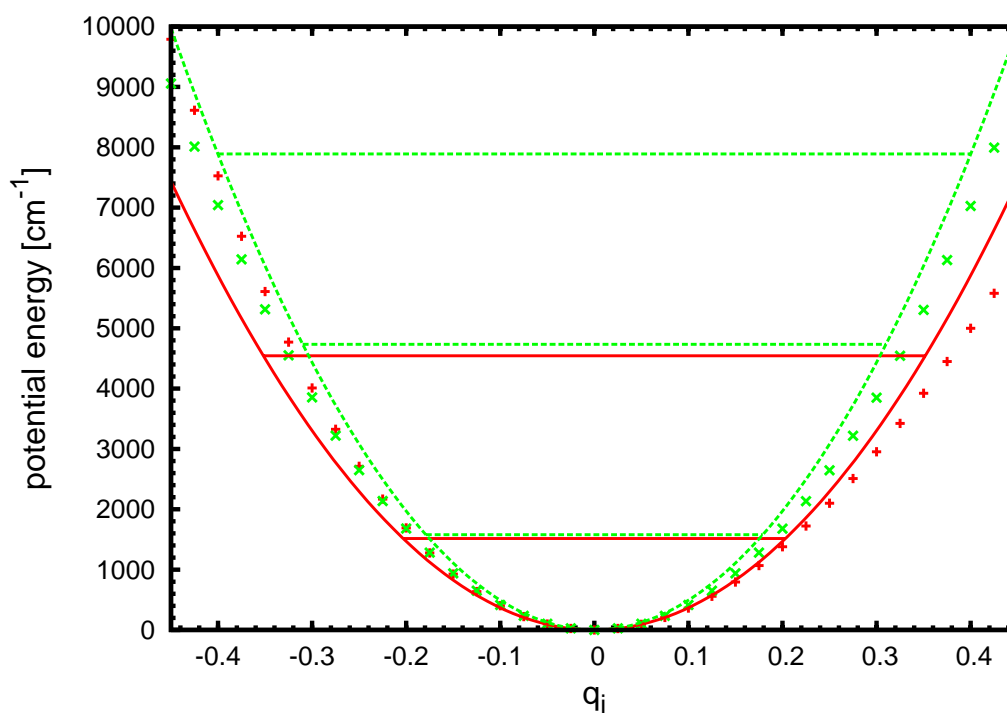


Figure 4.7: Plot of the approximated harmonic potential (lines) and harmonic oscillator levels for v_6 (red) and v_7 (green). The corresponding PES values are plotted as points. These modes are not harmonic. v_7 is symmetric but needs a higher than quadratic representation.

4.1.3 Morphing

The converged vibrational energies of a given potential energy surface have certain deviations from experimental values beyond the statistical error of the surface. Morphing is a method of changing the shape of the potential to fit a vibrational mode to a certain energy value and is therefore a coordinate transformation.

Assuming a purely harmonic potential, defined as $V(x) = ax^2$, a possible morph transformation is to add a constant offset to the coordinate: $x' = x + \varepsilon$. Inserting this into the harmonic potential delivers the morphed potential, still depending on the original variable, but with an additional factor: $V(x') = V(x + \varepsilon) = ax^2 + 2ax\varepsilon + a\varepsilon^2$. In this simple case the symmetric potential is modified with a constant offset and a linear term making the potential asymmetric. To preserve the symmetry of the potential, a transformation of the following form is more appropriate:

$$d'(i, j) = d(i, j) + \varepsilon(d(i, j) + a_0(i, j)) \quad (4.1)$$

a_0 is the equilibrium internuclear distance between atoms i and j . Methane has two types of internuclear distances, $C - H$ and $H - H$, therefore equation 4.1 splits into two equations with ε replaced with e_{xy} and e_{xx} and a_0 replaced with a_{xy} and a_{xx} , respectively.

Morphing can not improve the quality of the potential nor the resulting energies in terms of root mean square error or standard deviation, but for every independent morphing formula one mode can be morphed in a way that one single excitation level fits to some expected value. If the potential has the correct shape, other excitation levels of this mode may also improve. Since methane has four modes and two types of internuclear distances, only two of four modes can be adjusted. Improvements of other modes are not necessarily guaranteed by this procedure. Nevertheless, this method allows to improve the agreement between calculated excitation levels of single modes and experimental data.

The functional dependence of the CI energies of the fundamental excitations of all modes on the two ε 's were scanned separately. The results are plotted in figures 4.8 and 4.9. Modes n_4 and n_2 have a strong dependence on e_{xx} , while for modes n_1 and n_3 the dependence on e_{xy} is more pronounced. Hence, the functional dependencies seem linear in every case, a simple algebraic combination of both is possible to gain best agreement of the two selected modes.

$e_{xx} = 0.0008$ and $e_{xy} = 0.0040$ were chosen in order to optimize modes n_3 and n_4 . The corresponding energies are listed in table 4.3. The non-fitted mode n_1 is also in an excellent agreement with the experiment. This was obtained with additional effort in the selection for the PES fitting parameters. n_1 has a similar dependence on the morphing parameters as n_3 . Therefore, a difference of slightly above 100 cm^{-1} in the normalmode frequencies of these modes would result in the correct ratio of the CI energies. As presented in 3.1.2 there are parameters λ and a acting as truncation parameters in the PES. These values were changed to construct a PES

Table 4.3: Comparison of morphed CI energies of the fundamentals with experimental data [10].

$E_{Exp} [\text{cm}^{-1}]$	$E_{Morph} [\text{cm}^{-1}]$	rel. err.
1310,8	1311,01	1,63E-04
1310,8	1311,06	1,98E-04
1310,8	1311,09	2,25E-04
1533,3	1524,85	-5,51E-03
1533,3	1524,88	-5,49E-03
2916,5	2917,22	2,47E-04
3019,6	3019,22	-1,26E-04
3019,6	3019,45	-4,82E-05
3019,6	3019,55	-1,79E-05

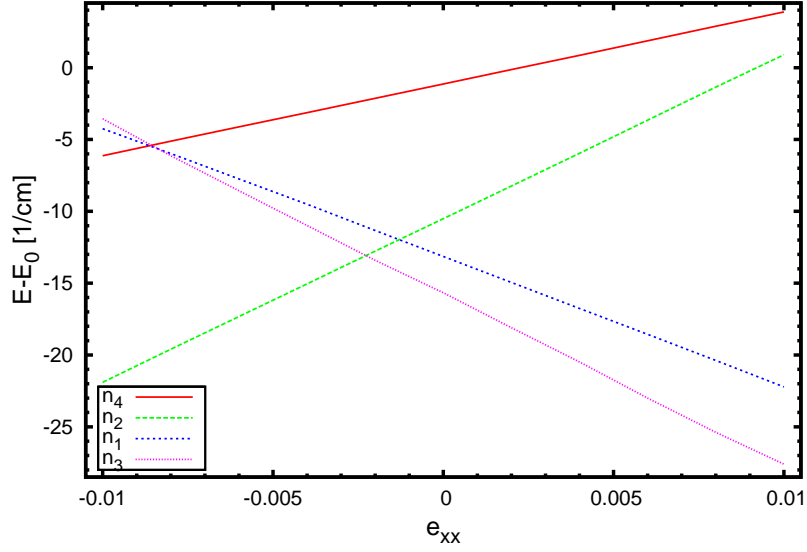


Figure 4.8: Dependence of the deviation of fundamental excitation energies from experimental values E_0 [10] on the morphing parameter e_{xx} .

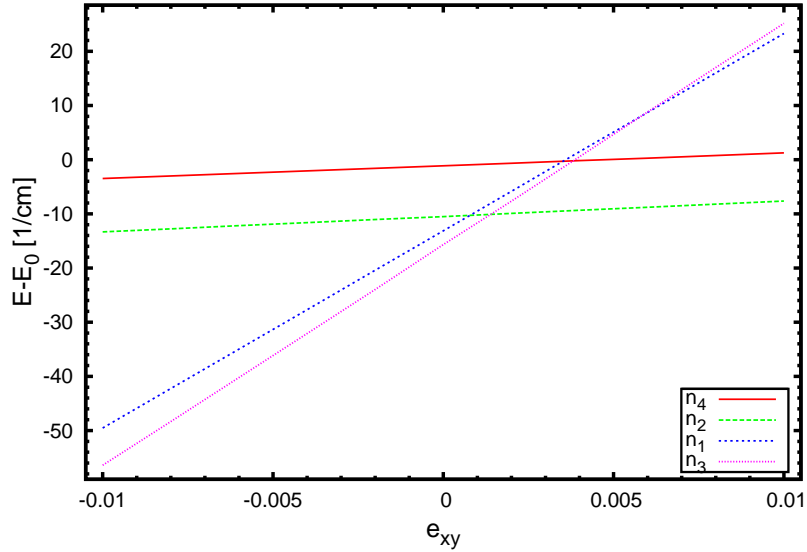


Figure 4.9: Dependence of the deviation of fundamental excitation energies from experimental values E_0 [10] on the morphing parameter e_{xy} .

according to this constraint. Nevertheless, it was not possible to adjust n_2 to the experimental values, because the relative error of this mode compared to experimental results is one order of magnitude higher than that of the others. This illustrates that morphing can improve matching of specific frequencies, but there is no global gain of accuracy from this procedure.

Other shortcomings of the morphing are the following: Because the normalmode vectors are partly mis-oriented (see 4.1.1) they do not reproduce the correct potential and its symmetry along the normalmode cuts. This can not be overcome by the morphing procedure. Also, for higher excitations incorrect energy splitting for the degenerated modes occurs. Since the consistency can not be guaranteed, there are no morphed energies used in this work.

4.1.4 Convergence

MULTIMODE uses a n -body expansion basis to describe the electronic potential. The quality of the results improves for a higher order expansion. The procedure is converging with increasing expansion order, so a threshold can be defined and a limit for the expansion can be found, where the variance of the resulting energies is lower than the threshold for every higher order term. The convergence threshold has to be determined by a compromise between quality and computational effort. Figure 4.10 shows the computing times and the memory used by MULTIMODE for different basis sets for a vibrational calculation. The figure can be interpreted in two ways. First, the dependence on the sum of the quanta for a given coupling can be seen, which is of quadratic nature. The dependence on the coupling for a certain sum of quanta is also identifiable and is quadratic, too. Although a practical limitation for memory usage is not reached in the vibrational case, a runtime of over 10000 seconds, almost 3 hours, is already critical, if one takes into account, that the rotational dependency is not included. A closer look on runtimes and memory consumption is presented in section 4.1.5.

The convergence behavior is shown in figure 4.11. A convergence with respect to the maxsum quanta can be reached for every mode coupling, but this is not a global convergence. This is reached, if a convergence for the mode coupling takes place. The 2-mode and 3-mode basis sets are not converged. The variance between 4-mode (4mr) and 5-mode (5mr) representations are of the order of $1 \cdot 10^{-4}$ or less than 2 cm^{-1} for every sumquanta. The variance between 4mr7 and 5mr7 is less than 0.3 cm^{-1} . This can be considered as well converged.

The convergence of low energy states does not guarantee automatically the convergence of higher energy states. Therefore, the 185th to 220th state have been compared for 4mr7, 4mr8 and 5mr7. Table 4.4 shows the energies and their relative deviation to the 5mr7 values. The energy of the 220th vibrational state is about 6100 cm^{-1} and is the highest vibrational level used in this work. The largest deviations to the 5mr7 in this block are $4.8 \cdot 10^{-3}$ and $4.48 \cdot 10^{-3}$ respectively. The 4mr7 and 4mr8 basis sets are considered as sufficient for this work.

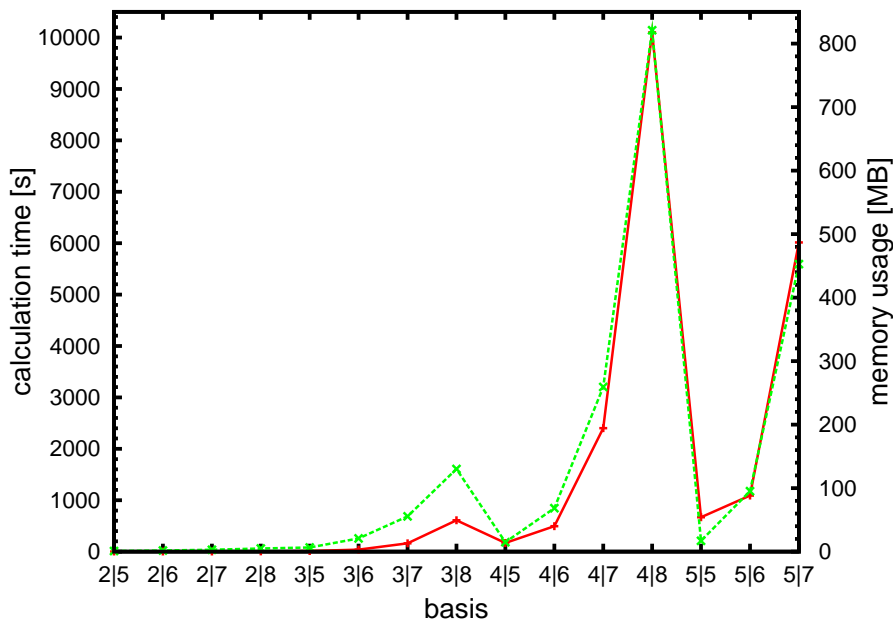


Figure 4.10: Dependence of computing time (red, straight line) and memory usage (green, dashed line) of expansion parameters for $J = 0$ and 25 CI energies calculated. $x|y$ means x -mode coupling with maximal sumquanta of y .

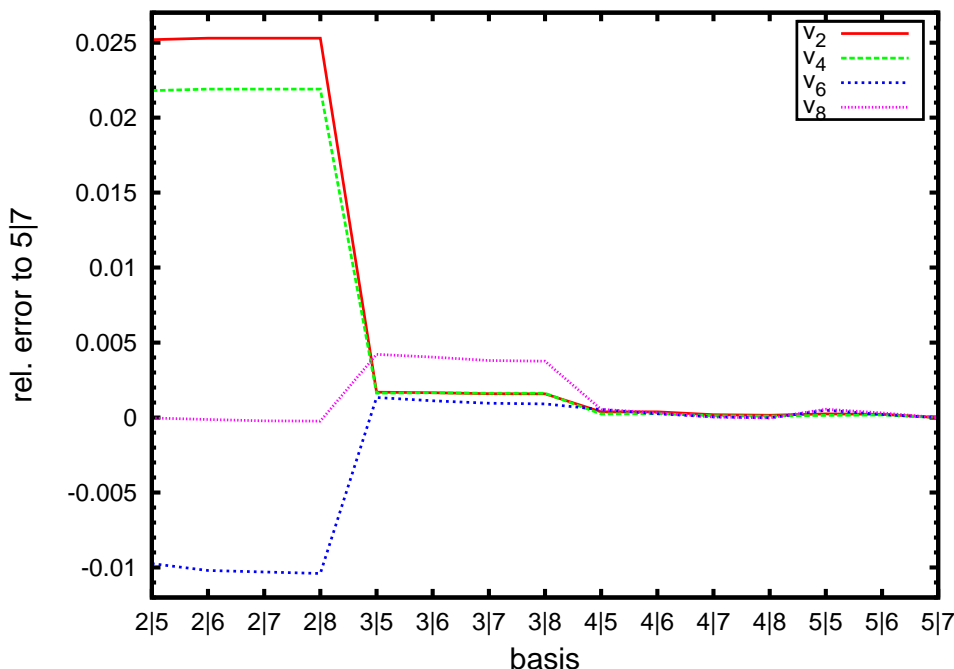


Figure 4.11: Relative deviation from 5-mode coupling calculation with MAXSUM=7 for different fundamental excitations. $x|y$ means x -mode coupling with maximal sumquanta of y .

4.1.5 Computational effort

The computational effort is a crucial factor limiting the level of theory which still can be used while having an acceptable runtime and memory usage. The dependence of the runtime and memory usage for the vibrational problem on the mode representation and the expansion order, expressed by the MAXSUM quanta, has been already explored in section 4.1.4, see figure 4.10. For this work mainly rovibrational problems are calculated. During an exact rotational calculation, first the vibrational problem is solved and then the final vibrational CI energies are printed for every projection of J , causing a linear increase of computing time, because a matrix diagonalization has to be done every time. This is the most time consuming part for vibrational calculations. The size of the vibrational CI matrix does not depend on the rotational quantum number, therefore the memory usage is not changing significantly. The final vibrational results are multiplied with the rotational function. For this, the rotational matrix is diagonalized. Its size is the number of CI energies per projection times the number of projections, giving a dependence for memory usage and runtime to the number of states to be calculated. This limits the number of vibrational states calculated for higher J 's.

In figure 4.12 the runtimes of the final rovibrational calculations done for this work are plotted. Exact calculations with 4mr8, dataset 1, and 4mr7, datasets 2 to 10, were done. The slope for 4mr7 is much flatter than for the 4mr8 calculations. 4mr8 calculations were done only with 220 CI energies per projection and are therefore comparable. Although the MULTIMODE Manual [37] predicts a quadratic correlation, figure 4.12 implies a more linear one. The 4mr7 calculations were done with varying number of CI energies. This is because the upper limit for energy values were set to 6200 cm^{-1} and due to the higher rotational energies, less and less vibrational modes are under this limit, as can be seen in figure 4.14. Section 4.2 provides a further explanation. For $J > 30$ no vibrational excitations are below the limit and for $J > 34$ in addition not even the rotational ground state is below this limit. For large numbers of CI energies a reduction causes a drop of runtime, because the calculation of the rotational matrix is time consuming.

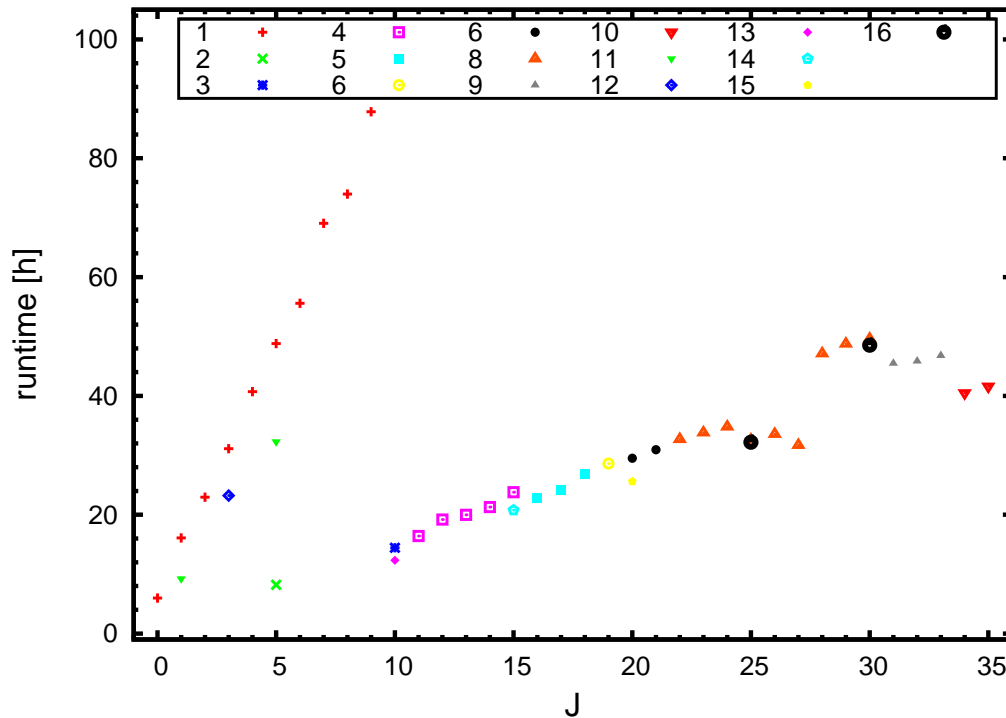


Figure 4.12: Runtime of MULTIMODE for rovibrational calculations with different settings: 1: 4mr8 with 220 CI energies per projection, 2: 4mr7 220, 3: 4mr7 157, 4: 4mr7 115, 5: 4mr7 95, 6: 4mr7 80, 7: 4mr7 76, 8: 4mr7 25, 9: 4mr7 6, 10: 4mr7 4, 11: 4mr8 220 adiabatic, 12: 4mr7 220 adiabatic, 13: 4mr7 157 adiabatic, 14: 4mr7 115 adiabatic, 15: 4mr7 76 adiabatic, 16: 4mr7 25 adiabatic

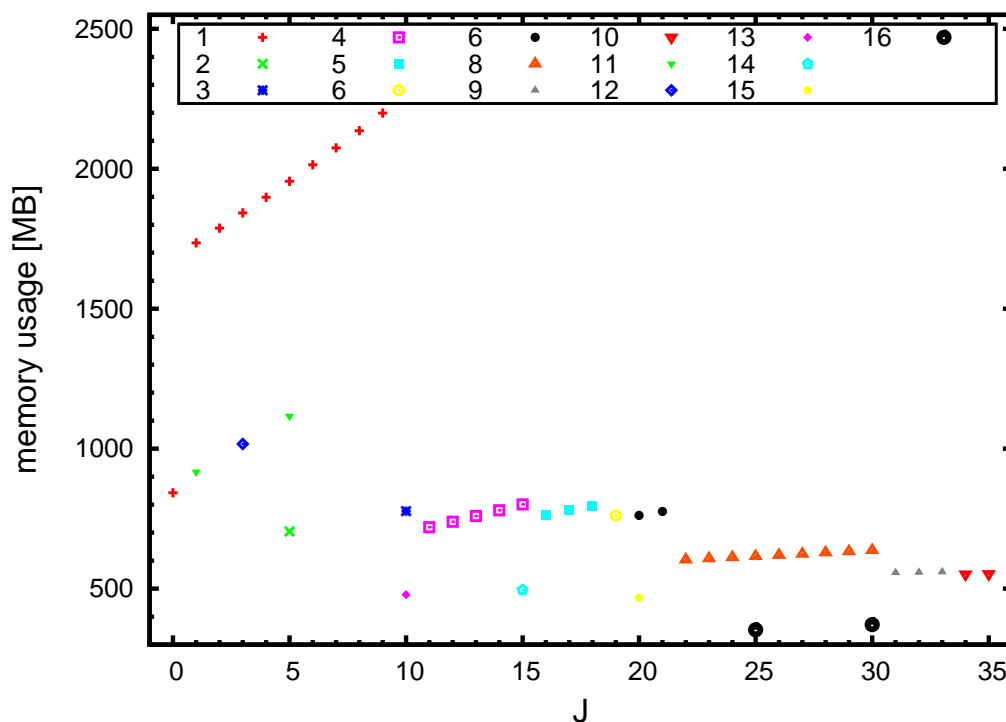


Figure 4.13: Memory usage of MULTIMODE for rovibrational calculations with different settings. The nomenclature is the same as in figure 4.12.

4.1 Tests

Table 4.4: List of vibrational modes 185 to 220. The experimental quantum numbers, symmetry and energies E [cm^{-1}] are listed. The computed energies E [cm^{-1}] for 4mr7 and 4mr8 are shown with relative error to 5mr7. One mode with wrong quantum number assignment is in this list and is marked-up.

Experimental			4mr7			4mr8		5mr7
n	Sym.	E	n	E	rel err	E	rel err	E
0301	F2	5867.66	0301	5853.14	5.81E-04	5849.98	4.03E-05	5849.74
0301	F2	5867.66	0301	5858.09	1.30E-03	5854.57	7.01E-04	5850.47
0301	F2	5867.66	0301	5858.72	1.34E-03	5855.42	7.80E-04	5850.86
0301	F1	5879.02	0301	5874.48	2.15E-03	5871.31	1.61E-03	5861.88
0301	F1	5879.02	0301	5875.16	2.23E-03	5872.23	1.73E-03	5862.09
0301	F1	5879.02	0301	5890.74	4.80E-03	5888.83	4.48E-03	5862.57
0301	F2	5894.12	0301	5891.00	2.68E-03	5889.30	2.39E-03	5875.24
0301	F2	5894.12	0301	5893.12	3.02E-03	5889.90	2.47E-03	5875.40
0301	F2	5894.12	0301	5893.92	3.09E-03	5892.00	2.76E-03	5875.78
0301	F1	5909.71	0301	5902.07	1.68E-03	5900.57	1.42E-03	5892.19
0301	F1	5909.71	0301	5915.49	3.94E-03	5913.70	3.63E-03	5892.30
0301	F1	5909.71	0301	5916.16	4.03E-03	5914.32	3.72E-03	5892.42
1200	A1	5971.52	1200	5917.95	2.75E-04	5915.65	-1.14E-04	5916.3
1200	E	5974.59	1200	5930.33	3.22E-04	5929.05	1.07E-04	5928.42
1200	E	5974.59	1200	5944.00	2.47E-03	5943.02	2.30E-03	5929.36
0020	A1	5968.09	1200	5944.91	5.02E-04	5943.39	2.46E-04	5941.93
0020	F2	6004.69	0020	5977.93	4.95E-04	5976.01	1.74E-04	5974.97
0020	F2	6004.69	0020	5978.57	5.31E-04	5976.73	2.23E-04	5975.40
0020	F2	6004.69	0020	5980.80	7.57E-04	5978.73	4.11E-04	5976.28
0020	E	6043.87	0020	6019.30	9.00E-04	6017.45	5.93E-04	6013.89
0020	E	6043.87	0020	6020.84	9.81E-04	6019.28	7.23E-04	6014.93
0210	F2	6054.64	0210	6028.17	8.63E-04	6027.14	6.93E-04	6022.97
0210	F2	6054.64	0210	6029.23	9.86E-04	6028.15	8.07E-04	6023.29
0210	F2	6054.64	0210	6030.47	1.10E-03	6029.13	8.80E-04	6023.83
0210	F1	6059.30	0210	6033.38	8.25E-04	6032.00	5.96E-04	6028.41
0210	F1	6059.30	0210	6035.08	9.91E-04	6033.55	7.38E-04	6029.10
0210	F1	6059.30	0210	6037.72	1.35E-03	6036.16	1.09E-03	6029.61
0210	F2	6065.32	0210	6050.20	2.33E-03	6049.59	2.23E-03	6036.16
0210	F2	6065.32	0210	6054.74	3.01E-03	6053.98	2.88E-03	6036.58
0210	F2	6065.32	0210	6057.69	3.45E-03	6056.78	3.30E-03	6036.88
0400	A1	6116.75	0400	6098.69	3.07E-05	6094.74	-6.17E-04	6098.50
0400	E	6118.62	0400	6099.68	1.68E-04	6095.57	-5.06E-04	6098.66
0400	E	6118.62	0400	6099.99	7.82E-05	6097.10	-3.96E-04	6099.52
0400	E	6124.17	0400	6101.33	1.72E-04	6098.52	-2.89E-04	6100.28
0400	E	6124.17	0400	6101.66	2.21E-04	6098.93	-2.27E-04	6100.32

For small number of CI energies this contribution is minor and the runtime is dominated by the vibrational calculations. Datasets 11 to 16 are adiabatic rotation calculations done with varying parameters. The runtime is significantly smaller for 4mr7 calculations compared with 4mr8 calculations. Especially for a small number of calculated energies this difference is negligible.

The memory usage is a second limiting factors for numerical calculations. The comparison between the $J = 0$ and $J = 1$ memory usage is splotted in figure 4.13 and shows a doubling of memory usage. For increasing J the dependence is stronger than linear. The memory usage for 4mr7 is a factor of roughly 2.5 smaller than for 4mr8 at $J = 5$, in addition the slope is significantly smaller. The dependence of memory usage on J is strongly determined by the number of calculated CI energies. While the steps between the 4mr7 datasets show the direct dependence of the number of energies the slope for a certain number of energies is smaller for less energies calculated. This is because the vibrational matrix size is constant for any given J , but the rotational matrix size is linearly dependent on J and the numbers of CI energies, as mentioned before. The adiabatic rotation calculations have a significant smaller memory usage. The difference between exact and adiabatic calculations is roughly of the size of the rotational matrix.

The calculations presented were done with AMD64 dual core processors @3 GHz with 4 GB of RAM per core, without parallelization. The 4-mode representation with maximal sumquanta of 8 is not treatable for $J > 10$, because the runtime increases over 3 days. The memory usage with more than 2 GB is large but treatable for 64-bit systems. The 4mr7 calculations are fast in comparison, without reaching any critical level of memory usage. To gain additional accuracy 5mr7 calculations are an alternative, with runtimes and memory usage between 4mr7 and 4mr8. The exact behavior would have to be examined. For this work 4mr8 were used for $J < 10$ calculations and 4mr7 for higher J s. The 4mr8 can be expected to be more robust for increasing J than 4mr7, but the computational time increases much faster and for $J > 9$ the runtimes exceed three days, enforcing due to practical considerations the use of 4mr7.

4.2 Rotational dependence for energies and dipoles

As discussed before the rovibrational energies have a quadratic dependence on J , as can be seen in figure 4.14. This leads to a reduction of vibrational states below a certain energy limit, in this case 6200 cm^{-1} , and in the end to an upper J , where no levels can be found anymore. This allows to calculate all rovibrational levels up to this limit and provide complete spectroscopic data within this region, as it has been done for this work with 52803 calculated energies in total, belonging to 30 bands. The further data processing had been done by integrating the 87 subbands.

In order to provide spectroscopic data a total number of 715500 dipole transition elements have been calculated, for 9 different J 's. This results in $30 \times 30 = 900$ different vibrational transitions. The provided dipole data is summed over all subbands and spatial directions. As shown in figure 3.2 for the transitions from fundamental excitations to the vibrational ground state the dependence of the dipole elements on J is either negligible or quadratic. In general, the dependence of the dipole moments on J can be estimated to be quadratic as shown by Buckingham [47]. A possible explanation for the other cases is based on their degeneration. The independent modes are threefold degenerated. For each of the three rotational axes occurs "rotational stretching" of the molecule, leaving it dynamically averaged spherical-symmetric. For the other modes preferred directions are existing with only minor dipole elements in the other directions. Hence the J dependence acts primarily for the preferred axis.

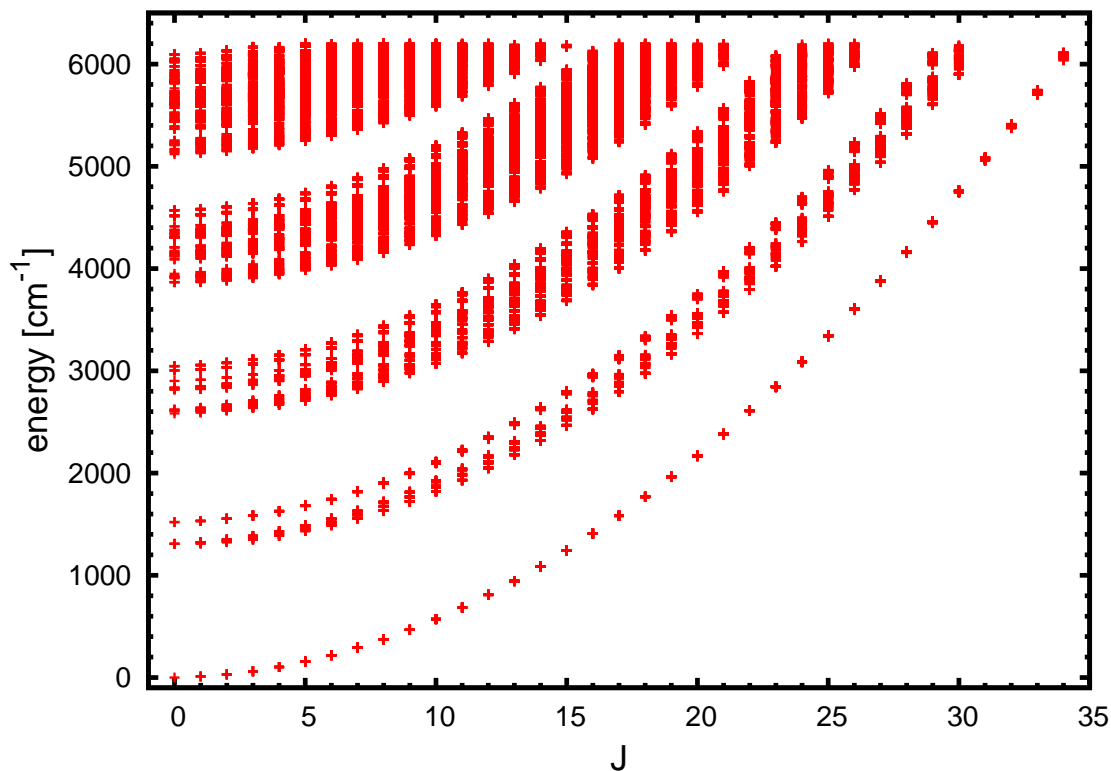


Figure 4.14: List of all rovibrational energy levels up to 6200 cm^{-1} . The energies are increasing quadratically with J and degenerated vibrations split.

4.3 Einstein coefficients

The final database provided by this work delivers Einstein coefficients A_{ij} as a function of wavenumbers. For methane the fundamental modes follow a relation as $n_1 \approx 2n_2 \approx n_3 \approx 2n_4$. Due to this, in the regular structured energy scaling the vibrational levels are divided into packets, called polyads. This can be seen in figure 4.14. Depending on the numbers of bands or levels the polyads are labelled Dyad ($\approx 1300 \text{ cm}^{-1} - \approx 1550 \text{ cm}^{-1}$), Pentad ($\approx 2500 \text{ cm}^{-1} - \approx 3100 \text{ cm}^{-1}$), Octad ($\approx 3850 \text{ cm}^{-1} - \approx 4600 \text{ cm}^{-1}$), Tetradecad ($\approx 5100 \text{ cm}^{-1} - \approx 6150 \text{ cm}^{-1}$) and so on. This scheme is also present in the A_{ij} spectrum. Figure 4.16 shows the complete spectrum of Einstein coefficients. The Dyad and Pentad regions show most pronounced peaks, whereas the ground state and the Tetradecad regions are only visible in logarithmic scale as done in figure 4.17. The A_{ij} spectrum shows the expected global features, but the details and the scaling depends on the specific calculation method (e.g. summation of sub-bands). HITRAN is a common spectroscopic database which can be used as a benchmark for the present data. It uses single lines with respect to subbands, but does not include every possible transition, only about 152000 lines for the given interval. The database obtained from this work includes every possible transition, but with merging of subbands into bands, resulting in 1.27 million database entries. A comparison can be delivered for processed data, as relative intensities, which are presented in section 4.4.

The calculation of spectra is of interest to understand the structuring. Figure 4.15 shows a detail of the database in the region of Pentads and Octads. The complete database is shown in red as a reference and examples for $\Delta J = -1, 0, +1$ are shown above. The spectrum has major peaks and at the base several rising plateaus. Although the different features can not be mapped to a certain type of transition an energy splitting for the different types is obvious. The plateaus are therefore results of the $\Delta J \neq 0$ transitions, while the main peaks should contain every type of transition.

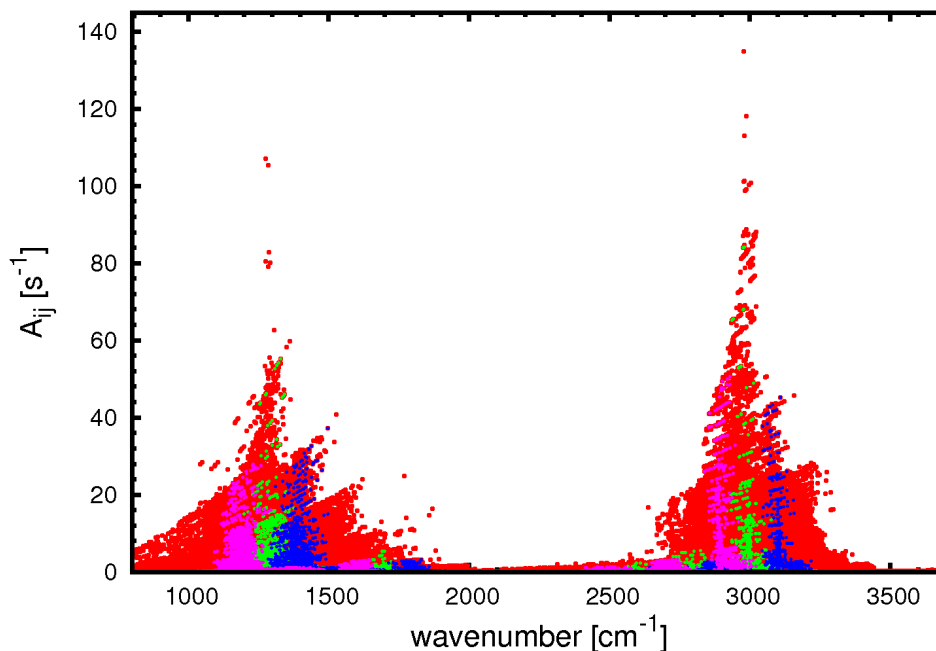


Figure 4.15: Einstein coefficients for different transitions in the interval $[800 \text{ cm}^{-1} : 3700 \text{ cm}^{-1}]$. Red: Whole spectrum. Green: $\Delta J = 0$ example with $J = 10$. Blue: $\Delta J = 1$ example with $J = 10 \rightarrow J = 9$, Purple: $\Delta J = -1$ example with $J = 9 \rightarrow J = 10$.

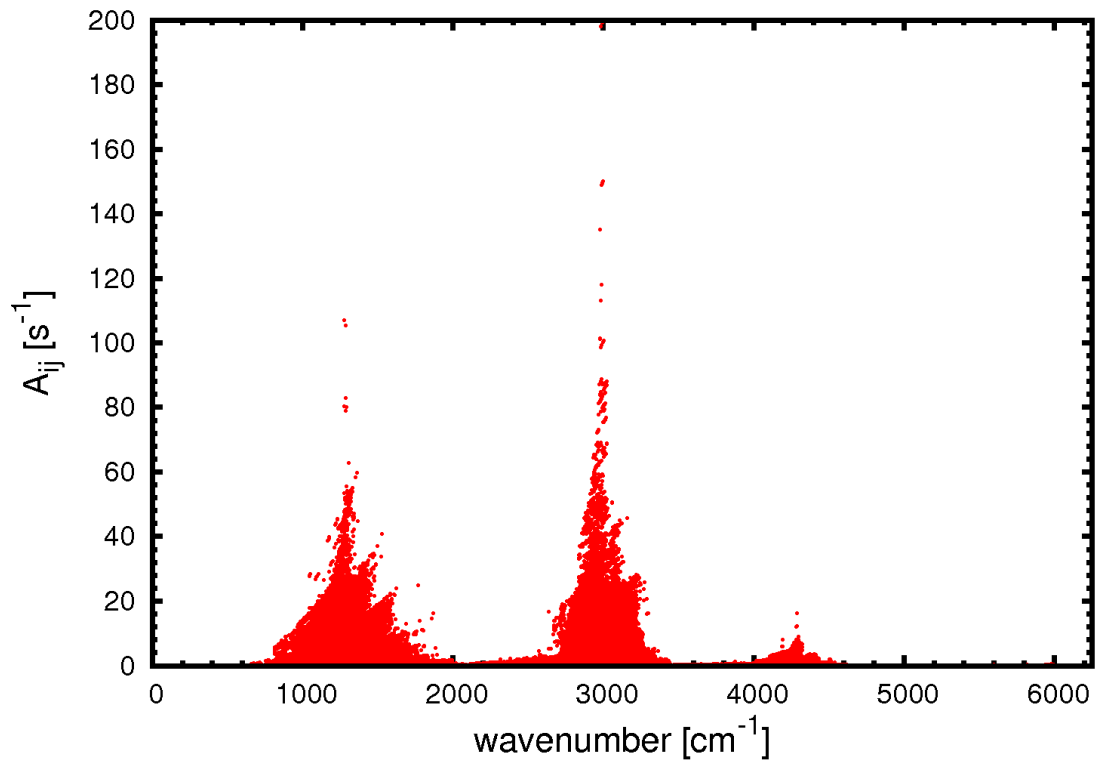


Figure 4.16: Complete set of Einstein coefficients up to 6200 cm^{-1} upper state energy in logarithmic scale.

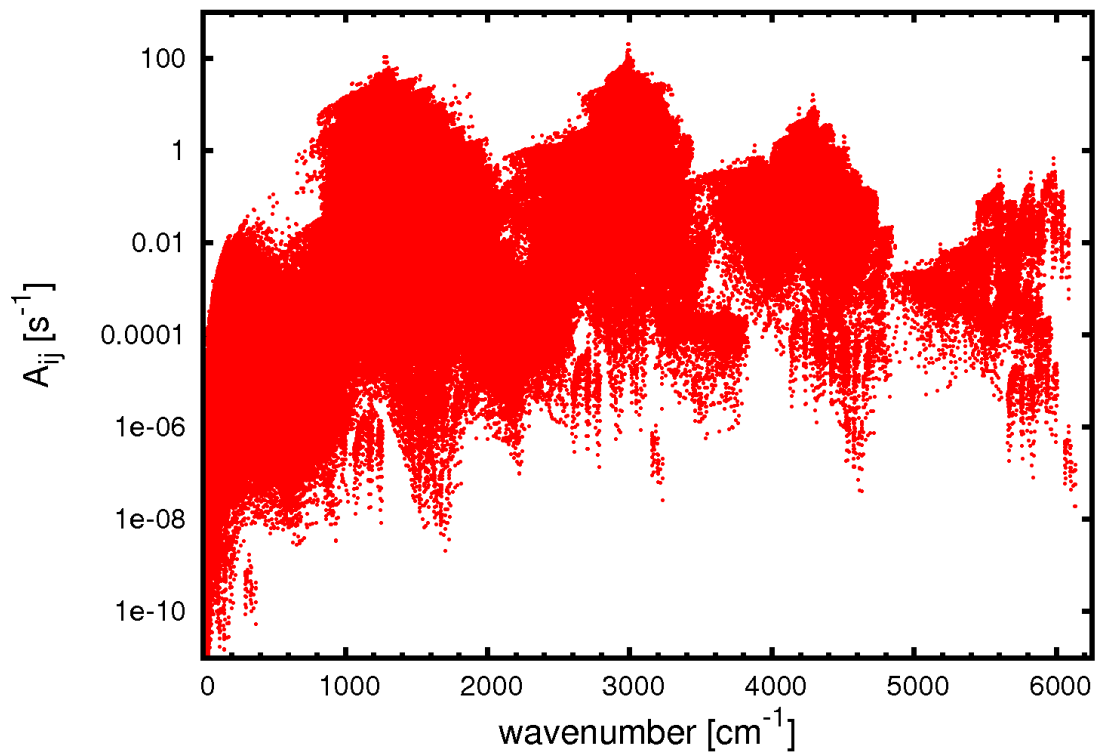


Figure 4.17: Complete set of Einstein coefficients up to 6200 cm^{-1} upper state energy with logarithmic scaling.

4.4 Spectra

A comparison of spectroscopic data without the problem of different data formats is possible with the calculation of simple temperature dependent emission spectra, where mainly relative intensities can be compared. For this purpose intensities of the form

$$I_{ij} \propto \frac{A_{ij}}{Q \cdot \left(e^{\frac{E_{\text{upper}}}{kT}} + 1 \right)} \quad (4.2)$$

where calculated for each line. Then the lines were projected to a grid of $\Delta E_{\text{wave}} = 1 \text{ cm}^{-1}$ using a $s = 1$ Lorentzian distribution to emulate line broadening. The projected lines are normalized in such a way, that the sum of the projected intensities on the grid is the same as the initial one. In cases where the relative spectra are wanted, an additional normalization is done to fix the sum of the intensities over the whole grid to unity.

4.4.1 Comparison of $J = 0$ lines for different evaluation methods

As explained before in 3.3, only averaged Einstein coefficients can be obtained with the chosen approach. The quality of the approximation can be tested for $J = 0$ transitions, for there the CI energies and the dipole matrix are calculated with the same wave function. Figures 4.18 show comparisons between intensity spectra produced with the $J = 0$ Einstein coefficients from the database and the non-compressed ones for $J = 0$. The ratio of the absolute intensities between exact and compressed is 1 : 0.96. This proves that the method used in this work to process the data is at least conserving the integral of the emission coefficients. Subfigures a) and b) are plotted without any apparatus function. In the region around 1300 cm^{-1} , shown in a), the exact method (red) has a major maximum and several minor maxima. These minor maxima are resulting from subband splitting. The green line shows the data from the database. Here the main maximum is reduced and additional intensity is transferred to the minor maxima. This happens because the energy averaging shifts the line center of the bands and acts stronger for higher excitations. A similar pattern can be found for the region around 3000 cm^{-1} in subfigure b). The other figures include an apparatus function simulated by a Gaussian distribution with halfwidth σ . For $\sigma = 3 \text{ cm}^{-1}$, the two curves are already similar and for $\sigma = 5 \text{ cm}^{-1}$ the lineshape gets very close. The major difference is a shift to lower energies for the composited data. This is a result of the energy averaging. The splitting of the vibrational bands causes mainly a lowering of energies. In cases where the measurement is technically limited to a resolution of 5 cm^{-1} or higher, the spectra have the same form with a small energy shift of about 10 cm^{-1} . For astrophysical applications the resolution of the produced data is high enough, because the astrophysical observation data is only of low accuracy in comparison to spectroscopic accuracies. An direct comparison with the HITRAN database is presented in 4.4.3.

4.4 Spectra

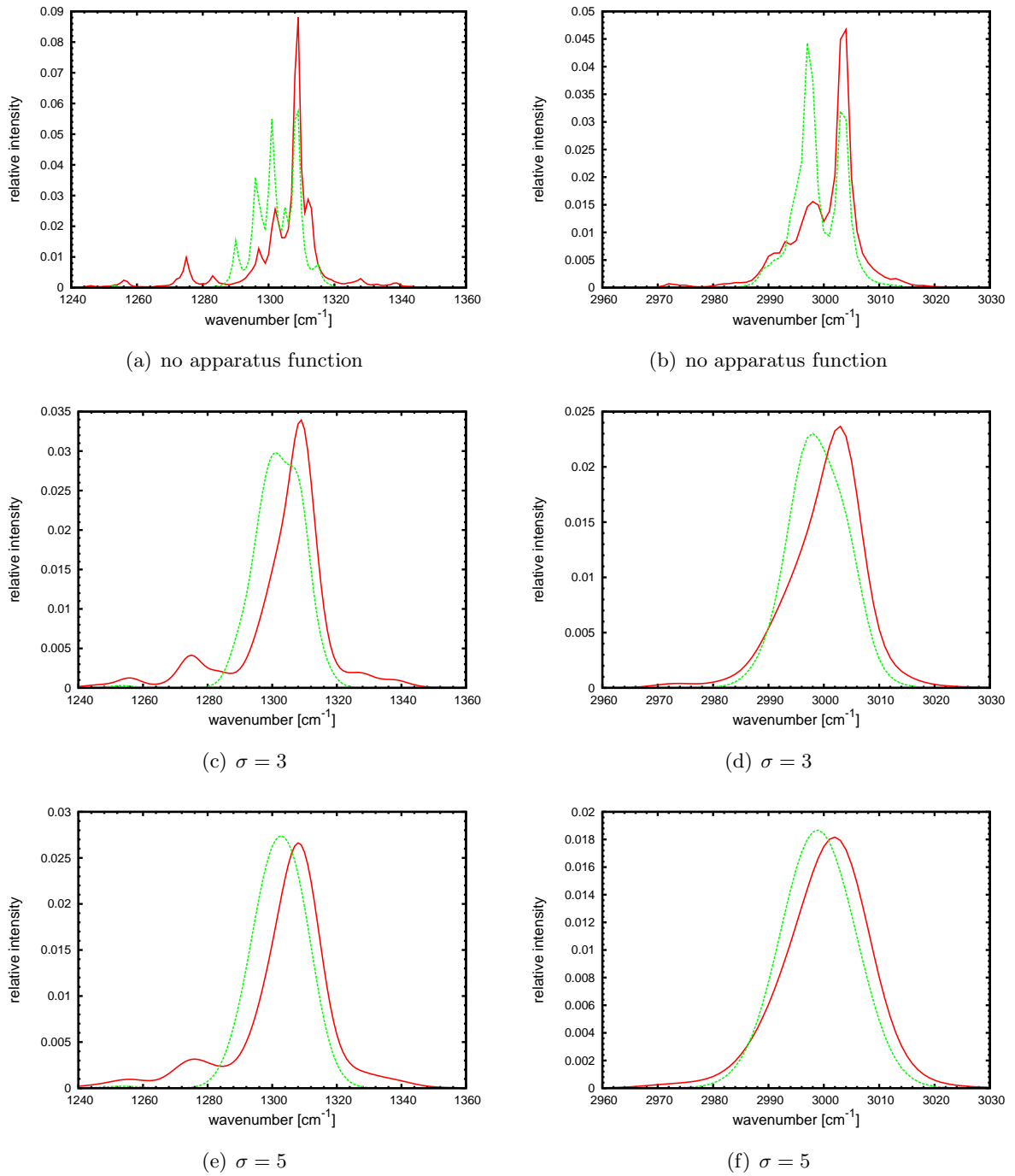


Figure 4.18: Relative intensity plots at 1000 K with Lorentzian line broadening with broadening parameter $s = 1 \text{ cm}^{-1}$ and different σ 's for the apparatus function (Gaussian). The red lines are direct $J = 0$ lines without any composition to bands or subbands. The green line is made from composited $J = 0$ band lines as used in the final database of this work. The red line can be interpreted as exact. The scaling factor of the absolute intensities between the methods is $1 : 0.96$. With a resolution of the measurement aperture of more than 3 cm^{-1} the composited spectrum is of sufficient accuracy besides a shift in the energies of about 10 cm^{-1} within the error range of the calculated energies.

4.4.2 Spectra for different temperatures

The spectra measured in astrophysics depend on the temperature of the light emitting body. Figure 4.19 shows relative intensities for the database for three different temperatures. The temperature dependence of the spectra is not related with the Einstein coefficients, but with the distribution function, see equation 4.2. From figure 4.19 it can be seen, that the relative intensity of regions with low linestrength is strongly dependent on the temperature, changing over several orders of magnitude. This shows the importance of a complete database including every possible transition.

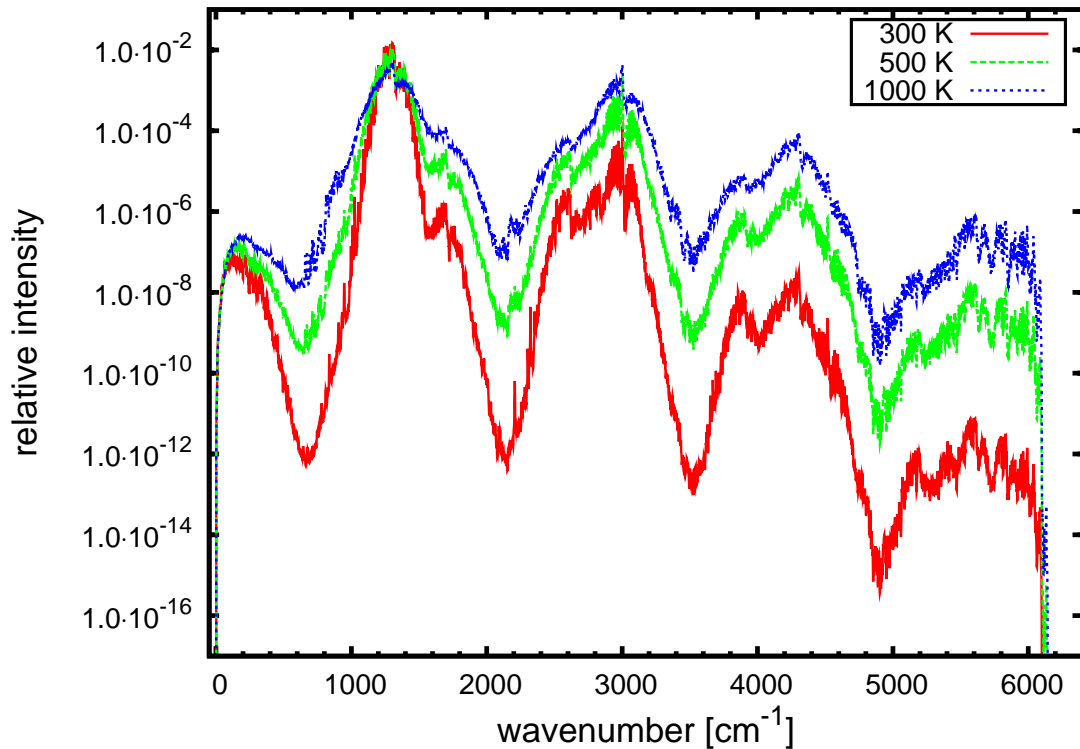


Figure 4.19: Relative intensities of transitions for different temperatures. For higher temperatures, the maximum moves to higher energies and the transmitting regions grow larger.

4.4.3 Comparison with HITRAN

A major benchmark for the quality of this work is the comparison with the HITRAN database. It includes about 187000 lines for methane with an upper limit of 10000 cm^{-1} . This is far less than provided by this work, although HITRAN allows single lines and not merged band lines. The precision of the single lines are higher though. For the astrophysical application the completeness is more important than the spectroscopic accuracy.

The comparison in figure 4.20 shows the same general structure for both databases. There are difference in the precise shape, but this is not critical, for this work was not meant to gain data with spectroscopic accuracy. Deviations are therefore expected and accepted. The HITRAN spectrum is not continuous, large regions are without data. This may cause integration errors for radiation transport. In contrast to that, the developed database has a continuous spectrum and meets consistency requirements.

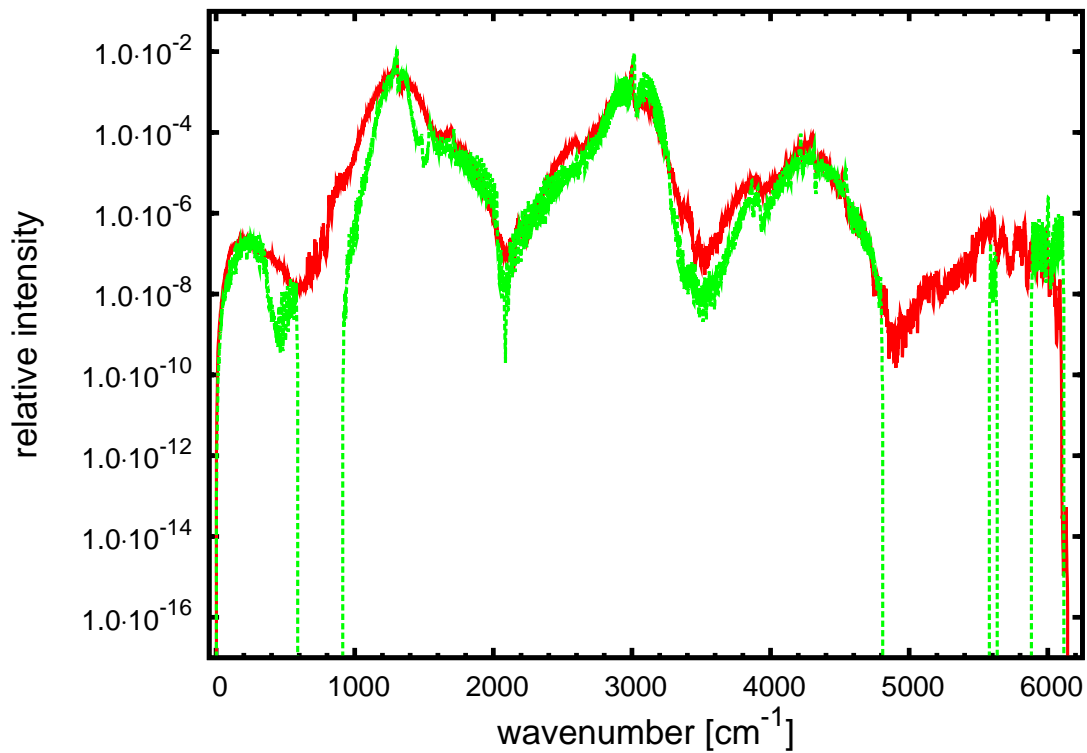


Figure 4.20: Comparison of 1000 K relative intensities between HITRAN and the database produced in this work. While no major deviations are obvious, it can be seen, that HITRAN does not cover the whole spectrum.

4.5 Astrophysical application

The common databases used for radiation transport calculations are patched with data from different sources. The consequence of this for the integration process is unknown. This work opens the chance to compare the common databases with one, which ensures consistency. A radiation transport calculation was performed by Prof Hauschildt for $T_{eff} = 1000\text{K}$ with $^{12}\text{CH}_4$ lines only. Figure 4.21 shows the radiation flux $\mathbf{F}_\lambda = \oint I_\lambda \mathbf{n} d\Omega$ emitted as a function of the wavelength. The flux has a smooth baseline as a function of temperature with absorption lines reducing the flux for certain wavelengths, depending on the atmospheric composition. Besides the current database (blue), fluxes for HITRAN (green) and GEISA (red) databases are shown. The GEISA database is the oldest one, being used mostly in the 1990's. It is outdated because of the small number of lines included. The GEISA database produces only few absorption lines leading to an insufficient adsorption. The comparison with HITRAN, which is a standard database nowadays, however shows similar absorption intensities over the whole range of wavelength. The absorption curve is broader for HITRAN.

The algorithm used in this work proved to be usable and of sufficient quality for astrophysics, despite the approximations, which had to be done. The agreement with the up-to-date HITRAN database is very good and in comparison to the older GEISA database it is much better. A mass-production of spectroscopic data for other molecules with the method used in this work is possible.

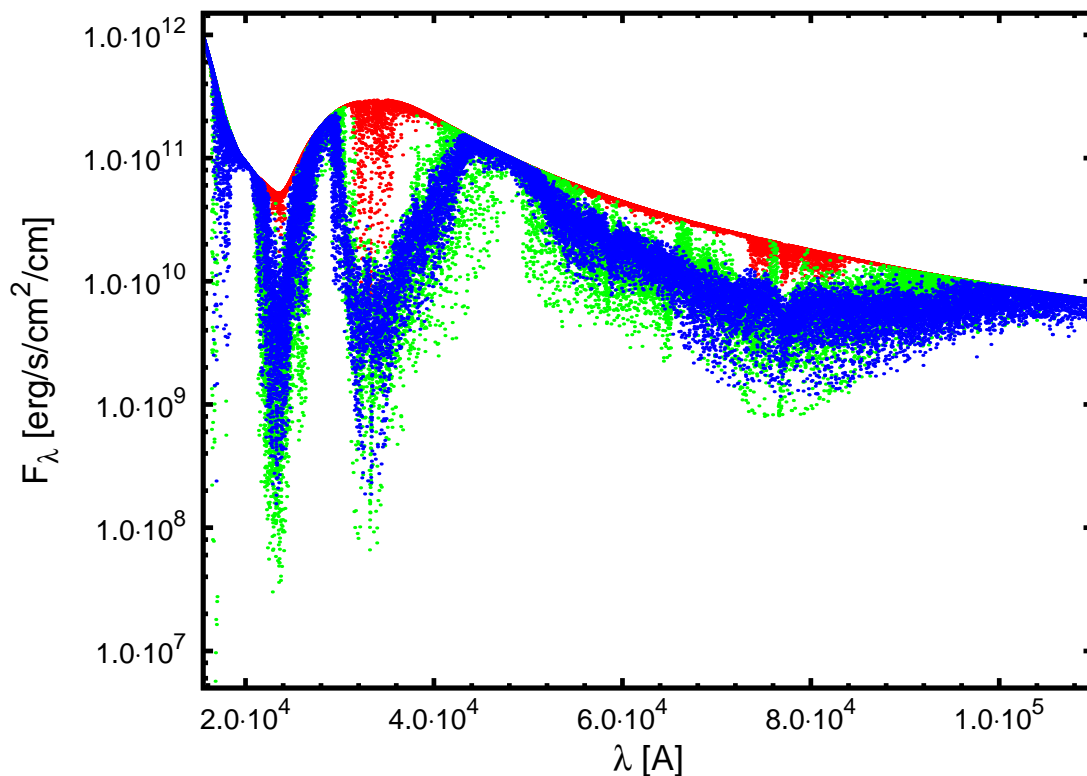


Figure 4.21: Radiative flux F_λ distribution dependent on wavelength for 1000 K. The absorption lines are $^{12}\text{CH}_4$ only. The databases shown are GEISA (red), HITRAN (green) and the one produced in this work (blue).

4.5.1 Perspective and improvements

Although the results the present work fulfill the accuracy demands of astrophysics, improvements can be done. An improved accuracy extends the possible applications of spectroscopic data obtained with the methods of the present work. Spectroscopic analysis are done in many fields of physics, e.g. plasma physics, with different accuracies.

A first step would be the improvement of the numerical conditioning of the PES. Calculations performed on different machines showed obvious deviations, smaller than the statistical error though and therefore not critical for the work. The next step is the improvement of the local fit of the PES with the addition of more datasets. A local fit nearer to *ab initio* data can deliver improved normalmode vectors leading to better CI expansion coefficients. The most time consuming, but most critical step is to calculate the dipole elements. The necessary changes in MULTIMODE to obtain the wave function for external processing and the writing of a code to calculate any dipole matrix element will be performed in a PhD thesis.

Chapter 5

Conclusion

The aim of the present work was to obtain spectroscopic data for astrophysics. These data are important for the analysis of the radiative behavior of substances. Methane was chosen for this task, as it is very often found in astrophysical measurements. The calculation of spectroscopic data requires several steps from the calculation of *ab initio* data to final Einstein coefficients. An algorithm for this was developed in this thesis. Several approximations, due to the restrictions of the codes used, had to be introduced. One of this is the merging of vibrational states at the level of bands and therefore losing the subband information. This turned out to introduce errors in the same order of magnitude as the statistical error of the potential energy surface. The errors are of the order of few percent. Since the energy dependence is cubic in the Einstein coefficients, these small errors are acceptable getting reduced further with this exponent. A more limiting factor was the calculation of dipole matrix elements. There the MULTIMODE package, which was used for these calculation, revealed severe shortcomings. The calculation of dipole matrix elements appeared to be limited to vibrational ones. For rovibrational motions these elements are lacking accuracy, because the rotational part of the wave function is not taken into account. A special adiabatic rotation approximated Hamiltonian was used to obtain the rigid rotor part of the rotational wave function. The K quantum number is not included. Due to this matrix elements for $\Delta J \neq 0$ and $\Delta K \neq 0$ could not be calculated. To handle this, the matrix elements had to be assumed to be independent of K . These necessary approximations were tested via a comparison of the spectroscopic data with the HITRAN database. It is an up-to-date database containing spectroscopic information built from several sources. The comparison showed a good agreement between the database obtained in this work and the HITRAN database. Despite the approximations, which had to be made the method resigned to be adequate with respect to the quality needed for astrophysics. The advantage of the database produced in this work is the guaranteed consistency of the data, because they are calculated using one single method. The results demonstrated the potential of the general ansatz. Spectroscopic data for astrophysics can be produced using the algorithm developed here. For applications with higher accuracy demands than astrophysics, improvements of the method have to be done, reducing the overall error.

Bibliography

- [1] Neptune, 27.04.2008. http://solarsystem.nasa.gov/multimedia/display.cfm?IM_ID=2424.
- [2] S.K. Leggett, M.S. Marley, R. Freedman, D. Saumon, M.C. Liu, T.R. Geballe, D.A. Golimowski, and D.C. Stephens. Physical and spectral characteristics of the t8 and later type dwarfs. *ASTROPHYSICAL JOURNAL*, 667(1):537 – 548, 2007.
- [3] L. R. Brown, D. C. Benner, J. P. Champion, V. M. Devi, L. Fejard, R. R. Gamache, T. Gabard, J. C. Hilico, B. Lavorel, M. Loete, G. C. Mellau, A. Nikitin, A. S. Pine, A. Predoi-Cross, C. P. Rinsland, O. Robert, R. L. Sams, M. A. H. Smith, S. A. Tashkun, and V. G. Tyuterev. Methane line parameters in hitran. *Journal of Quantitative Spectroscopy & Radiative Transfer*, 82(1-4):219 – 238, 2003.
- [4] L.S. Rothman, D. Jacquemart, A. Barbe, D.C. Benner, M. Birk, L.R. Brown, M.R. Carleer, C. Chackerian, K. Chance, L.H. Coudert, V. Dana, V.M. Devi, J.M. Flaud, R.R. Gamache, A. Goldman, J.M. Hartmann, K.W. Jucks, A.G. Maki, J.Y. Mandin, S.T. Massie, J. Orphal, A. Perrin, C.P. Rinsland, M.A.H. Smith, J. Tennyson, R.N. Tolchenov, R.A. Toth, J. Vander auwera, P. Varanasi, and G. Wagner. The hitran 2004 molecular spectroscopic database. *Journal of Quantitative Spectroscopy & Radiative Transfer*, 96(2):139 – 204, 2005.
- [5] A.R. Sharma, R. Schneider, U. Toussaint, and K. Nordlund. Hydrocarbon radicals interaction with amorphous carbon surfaces. *Journal of Nuclear Materials*, 363:1283 – 1288, 2007.
- [6] A.R. Sharma. *Atomistic modelling of hydrocarbons in plasma-wall interaction*. PhD thesis, University of Greifswald, 2008.
- [7] R. Schneider, A. Rai, A. Mutzke, M. Warriier, E. Salonen, and K. Nordlund. Dynamic monte-carlo modeling of hydrogen isotope reactive-diffusive transport in porous graphite. *Journal of Nuclear Materials*, 367:1238 – 1242, 2007.
- [8] A. Rai, P.N. Maya, R. Schneider, S.P. Deshpande, and M. Warriier. Dynamic monte-carlo modeling of hydrogen isotope diffusion in co-deposited layers. *Journal of Nuclear Materials*, 363:1272 – 1276, 2007.
- [9] Methane, 13.04.2008. <http://encyclopedia.airliquide.com/>.
- [10] X.G. Wang and T. Carrington. A contracted basis-lanczos calculation of vibrational levels of methane: Solving the schrodinger equation in nine dimensions. *Journal of Chemical Physics*, 119(1):101 – 117, 2003.
- [11] Demtröder. *Atome, Moleküle und Festkörper*, volume 3 of *Experimentalphysik*. Springer, 2005.
- [12] A. Messiah. *Quantenmechanik II*. de Gruyter, 1981.
- [13] F. Schwabl. *Quantenmechanik*. Springer, 6 edition, 2005.

-
- [14] L.D. Landau and E.M. Lifschitz. *Quantenmechanik*, volume III of *Lehrbuch der Theoretischen Physik*. Akademie-Verlag, Berlin, 9 edition, 1979.
- [15] R. Oppenheimer M. Born. Zur quantentheorie der molekeln. *Annalen der Physik*, 389(20):457–484, 1927.
- [16] F. Schwabl. *Quantenmechanik für Fortgeschrittene*. Springer, 6 edition, 2005.
- [17] M. D. Bertolucci D. C. Harris. *Symmetry and Spectroscopy: An Introduction to Vibrational and Electronic Spectroscopy*. Dover Publications Inc., November 1989.
- [18] L.D. Landau and E.M. Lifschitz. *klassische Mechanik*, volume I of *Lehrbuch der Theoretischen Physik*. Akademie-Verlag, Berlin.
- [19] Knowles P.J. et al. Werner, H.-J. *Molpro, version 2006.1, a package of ab initio programs*, 2006. see <http://molpro.net>.
- [20] M. Headgordon. Quantum chemistry and molecular processes. *Journal of Physical Chemistry*, 100(31):13213 – 13225, 1996.
- [21] Configuration interaction, 21.04.2008. http://en.wikipedia.org/wiki/Configuration_interaction.
- [22] R.J. Gdanitz and R. Ahlrichs. The averaged coupled-pair functional (acpf) - a size-extensive modification of mr ci(sd). *Chemical Physics Letters*, 143(5):413 – 420, 1988.
- [23] R.J. Gdanitz. A new version of the multireference averaged coupled-pair functional (mr-acpf-2). *International Journal of Quantum Chemistry*, 85(4-5):281 – 300, 2001.
- [24] X.C. Huang, B.J. Braams, and J.M. Bowman. Ab initio potential energy and dipole moment surfaces for h5o2+ (vol 122, art no 044308, 2005). *Journal of Chemical Physics*, 127(9):099904, 2007.
- [25] A.R. Sharma, J.Y. Wu, B.J. Braams, S. Carter, R. Schneider, B. Shepler, and J.M. Bowman. Potential energy surface and multimode vibrational analysis of c2h3+. *Journal of Chemical Physics*, 125(22):224306, 2006.
- [26] Bai Z. Bischof C. et al. Anderson E., editor. *LAPACK User's Guide*. SIAM, Philadelphia, 3rd edition, 1999.
- [27] Derksen H. and Kemper G. *Computational Invariant Theory*. Springer, 2002.
- [28] W. Bosma, J. Cannon, and C. Playoust. The magma algebra system .1. the user language. *Journal of Symbolic Computation*, 24(3-4):235 – 265, 1997.
- [29] S. Carter, H. M. Shnyder, and J. M. Bowman. Variational calculations of rovibrational energies of ch4 and isotopomers in full dimensionality using an ab initio potential. *Journal of Chemical Physics*, 110(17):8417 – 8423, 1999.
- [30] S. Carter, J.M. Bowman, and N.C. Handy. Extensions and tests of 'multimodes': a code to obtain accurate vibration/rotation energies of many-mode molecules. *Theoretical Chemistry Accounts*, 100(1-4):191 – 198, 1998.
- [31] S. Carter, S.J. Culik, and J.M. Bowman. Vibrational self-consistent field method for many-mode systems: A new approach and application to the vibrations of co adsorbed on cu(100). *Journal of Chemical Physics*, 107(24):10458 – 10469, 1997.

- [32] S. Carter and J. M. Bowman. The adiabatic rotation approximation for rovibrational energies of many-mode systems: Description and tests of the method. *Journal of Chemical Physics*, 108(11):4397 – 4404, 1998.
- [33] J. Y. Wu, X. C. Huang, S. Carter, and J. M. Bowman. Tests of multimode calculations of rovibrational energies of ch4. *Chemical Physics Letters*, 426(4-6):285 – 289, 2006.
- [34] A. Chakraborty, D. G. Truhlar, J. M. Bowman, and S. Carter. Calculation of converged rovibrational energies and partition function for methane using vibrational-rotational configuration interaction. *Journal of Chemical Physics*, 121(5):2071 – 2084, 2004.
- [35] J. M. Bowman. The self-consistent-field approach to polyatomic vibrations. *Accounts of Chemical Research*, 19(7):202 – 208, 1986.
- [36] R.J. Whitehead and N.C. Handy. Variational calculation of vibration-rotation energy-levels for triatomic-molecules. *JOURNAL OF MOLECULAR SPECTROSCOPY*, 55(1-3):356 – 373, 1975.
- [37] J. Bowman S. Carter. *Manual for Multimode*, 3.4 2/99 edition. <http://www.chemistry.emory.edu/faculty/bowman/multimode/>.
- [38] J. K. G. Watson. Simplification of molecular vibration-rotation hamiltonian. *MOLECULAR PHYSICS*, 15(5):479 – &, 1968.
- [39] M.R. Aliev D. Papoušek. *Molecular Vibrational-Rotational Spectra*. Elsevier Scientific Publishing Company, 1982.
- [40] S. Carter and J. M. Bowman. Variational calculations of rotational-vibrational energies of ch4 and isotopomers using an adjusted ab initio potential. *Journal of Physical Chemistry A*, 104(11):2355 – 2361, 2000.
- [41] A. Hansson and J.K.G. Watson. A comment on hönl-london factors. *JOURNAL OF MOLECULAR SPECTROSCOPY*, 233(2):169 – 173, 2005.
- [42] J.M. Hure and E. Roueff. Analytic representations of rovibrational dipole matrix elements for the co molecule and its isotopomers. *ASTRONOMY & ASTROPHYSICS SUPPLEMENT SERIES*, 117(3):561 – 568, 1996.
- [43] S Carter, J Senekowitsch, NC Handy, and P Rosmus. Calculations of the ro-vibrational absorption transition-probabilities in triatomic-molecules. *MOLECULAR PHYSICS*, 65(1):143 – 160, 1988.
- [44] F. London H. Hönl. über die intensitäten der bandlinien. *Zeitschrift für Physik*, 33, 1925.
- [45] D.R. Lide E.A. Cohen and G. Trigg. *A Physicist's Desk Reference*, chapter 15 Molecular Spectroscopy and Structure. AIP Press, third edition edition, 2000. by P.F. Bernath.
- [46] E. Cantarella, F. Culot, and J. Lievin. Ab initio calculation of vibrational dipole-moment matrix-elements .1. methods of calculation and diatomic test systems. *PHYSICA SCRIPTA*, 46(6):489 – 501, 1992.
- [47] A. D. Buckingham. Temperature-dependent chemical shifts in the nmr spectra of gases. *The Journal of Chemical Physics*, 36(11):3096–3096, 1962.

Bibliography

Acknowledgements

At the very end of this work I would like to express my gratitude to all who helped me during the last eight months. First of all I want to thank my supervisor Dr. Ralf Schneider for his support, patience and good advices. I am deeply grateful having had such a caring supervisor. The help of Dr. Amit Rai Sharma and Dr. Bastiaan Braams was irreplaceable, especially in the first months, and therefore I am indebted to them. I also want to mention Prof. Joel Bowman whose deep knowledge of quantum chemistry was very enlightening.

I want give thanks to all group members here in Greifswald for always being helpful, patient and for the good working atmosphere.

Last but not least I want to thank my girlfriend, friends and family being patient with me during the last months.

Name, Vorname: Warmbier, Robert

geboren: 28.08.1984

Matrikelnummer: 105658

Korrespondenzanschrift: Ernst-Thälmann-Ring 8a, Whg 7, 17491 Greifswald

Ernst-Moritz-Arndt Universität Greifswald

Zentrales Prüfungsamt

Rubenowstraße 2, 17487 Greifswald

Bearbeiterin: Frau Sanne

Erklärung zur Diplomarbeit

Ich versichere, dass ich die anliegende Diplomarbeit mit dem Thema:

Spectroscopic data for astrophysics

selbstständig verfasst und keine anderen als die angegebenen Hilfsmittel verwendet habe.

Greifswald, 29. April 2007

Robert Warmbier